Experimental Study of Performance Degradation of a Rotating System in the NASA Lewis RC Icing Tunnel

Final Technical Report

NASA Grant NCC 3-132

02/21/89 to 06/28/91

Submitted by

Dr. Kenneth Korkan

Department of Aerospace Engineering

Texas A&M Research Foundation
Box 3578
College Station, TX 77843

Effects of Simulated Icing Conditions on Lift, Thrust, and Torque Variations of a Model Helicopter Rotor as a Function of Time*

L.A. Eagleson**

Texas A&M University
College Station, TX 77843

Abstract

The Helicopter Icing Consortium (HIC)† conducted one of the first U.S. tests of a heavily instrumented model in the controlled environment of a refrigerated tunnel (1). In the Icing Research Tunnel (IRT) at NASA Lewis Research Center (NASA LERC), ice was accreted on the main rotor blade of the BMTR-1 Sikrosky model helicopter under a variety of environmental conditions, such that liquid water content (LWC) and volume mean droplet diameter (VMD) ranges reflected the Federal Aviation Agency and Department of Defence icing condition envelopes (1). This report gives the correlated results of the data provided by NASA LERC. The method of statistical analysis is discussed. Lift, thrust, and torque coefficients are presented as a function of icing time, as correlated with changes in ambient temperature, LWC, and VMD. The physical significance of these forces is discussed.

Introduction

A majority of the U.S. military and civil helicopters in use today do not have clearance to operate in forecast icing conditions, or have a strictly limited clearance, due to the extreme sensitivity rotors display under ice accretion conditions. Currently the industry is lacking reliably adequate rotor deicing systems, and present all-weather certification of U.S. military and civil helicopters relies heavily upon flight testing in natural icing conditions, which is an expensive, potentially hazardous, and time-consuming process. Therefore U.S. helicopter manufacturers, in order to increase their all-weather capabilities, have expressed a desire for alternate methods of data

* This research is supported by NASA Lewis Research Center Grant NCC 3-132

** Graduate Reseach Assistant.

† HIC is comprised of NASA Lewis Research Center, Texas A&M University, Bell Helicopter Textron, Boeing Helicopter, McDonnell Douglas Helicopters, and Sikorsky Aircraft.

acquisition to be used in obtaining FAA certification. Prior to the OH-58 Tail Rotor Rig test at NASA LERC, only the French had conducted any icing wind tunnel testing of a scaled rotor (3). Their data compared favorably with full-scale natural icing flight test data, and indicated that icing tunnel testing would prove to be a viable method of collecting iced rotor performance data (4, Appendix B). The promising results obtained in the ONERA Wind Tunnel by Guffond (3) was instrumental in the formation of the HIC, the OH-58, and the Sikrosky BMTR-1 testing.

Data Acquistion

Experimental data was obtained through a dynamic data acquisition system, a safety of flight system, and a number of other measurement and cataloguing techniques. Spray times, temperature and shedding event times were recorded, and each run was video-taped to provide a time-history of the ice accretion and shedding. Appendix C contains photographs of the ice accreted along the leading edge of the rotor blades during testing and lists the conditions under which the ice shapes were formed.

Data Analysis

Ratio of coefficients of torque, lift, and thrust to solidity, i.e., C_Q/σ, C_L/σ, and C_T/σ, respectively, were plotted versus icing time for correlation parameters of temperature, LWC, VMD. Early analyses of the data (5) indicated that shaft angle, θ, had little effect on torque, lift, and thrust response to icing conditions. Therefore two sets of data were correlated; one set includes θ, the other does not assume θ to be a significant variable.

Data files were received in Lotus format and plotted using the graphics package Grapher, readily available in the Department of Aerospace Engineering at Texas A&M University. The data was corrected for icing start time before plotting. In the original files, data was obtained before the initiation of icing conditions, therefore when data was correlated, points were taken beginning at the icing start time. The last twenty to thirty seconds of data taken indicate the response of the rotor to a decrease in ice accretion as the spray rig was shut off, referred to as the rotor's "post cloud behavior (2)." The standard deviation of the statistical variables LWC, VMD, and temperature was kept to a minimum when choosing data sets for analysis; however, no other restrictions were placed on the chosen sets. It was found that including θ as a statistical variable greatly reduced the variety of icing runs which could be grouped for analysis. Effort was made to use as many different sets of icing data as possible in order to obtain a representational subset of the complete data taken.

Physical Significance

Helicopter rotor performance is highly sensitive to ice accretion; lift, thrust, and torque will vary with the type of ice accreted, the variation of ice growth along the span of the blades, and the amount and location of shed ice. Thus it is important to understand the characteristics of ice accretion and the physical properties of the accreted ice in order to begin to describe rotor performance variations.

Ice will grow nonuniformly along the span of a blade as a function of local velocity variation and local aerodynamic heating effects. The smooth rime ice, which in some experiments has been shown to actually increase the performance of a blade under certain conditions, increases in thickness as a function of velocity. However, aerodynamic heating effects increase in significance as a function of velocity also, and can raise the surface temperature such that the rime ice shape is transformed into the more detremental double-horn shape of glaze ice (2).

Rime ice is associated with smaller droplets, lower LWC values, and temperatures below 14 degrees Fahrenheit. These smaller droplets are more likely to be deflected around the airfoil, resulting in a small impingement zone near the leading edge. Glaze ice forms at temperatures between 14 degrees Fahrenheit and freezing and has a density nearer to that of water than rime ice. As droplet size and density increases, the impingement limit moves farther back on the airfoil of the blade, causing a greater area to be influenced by the accretion process.

The shedding process plays an important role in the outcome of an icing encounter. If ice is shed from a propeller late in the accretion process, the shed ice may cause damage to the fuseage or may be injested by intakes. Heavily accreted blades which shed nonuniformly may experience unbalance, which results in high vibratory loads on the rotor. The goal of deicing systems, then, is to force shedding early in the accretion process, before significant decreases in lift and thrust occur, and before the mass (thus energy) of the shed ice becomes a hazard to the aircraft.

Torque

In all cases tested, torque rose as a function of icing time. For both sets of data, C_Q/σ increases for increasing VMD, as shown clearly in Figure 1. Figure 2 shows a no-shedding case at VMD=15μm. Rotor torque decreases slightly for minor shedding, and exhibits more pronounced changes when large areas of accreted ice are shed. In almost cases, some residual ice will be seen after shedding.

Increase in LWC increases C_Q/σ as expected, as seen in Figures 3 and 4. Note the overlapping which occurs in Figure 3 that does not in Figure 4, suggesting that LWC plays less of a role at higher temperatures on the affects of torque. The effects of temperature at two different shaft angles are shown in Figures 5 and 6. As temperature increases, the torque needed by the rotor to maintain a contant rotational velocity decreases, indicating that some melting and/or shedding has occured on the blades.

Figure 7 clearly indicates the effects of negative and positive θ on torque. Both show steady increasing functions with icing time, but the shift in value of C_Q/σ is approximately 0.28 throughout the icing time, where $C_Q/\sigma(\theta$ =-6.5) > $C_Q/\sigma(\theta$ =+2.4).

Lift

Lift was shown to decrease with icing time for all parameters analyzed. It is not smoothly decreasing, but an overall oscillatory decrease. At the start of an icing encounter, lift will decrease rapidy due to the roughness induced by the initial ice accreted (2). Figures 8 and 9 show CL/σ as a function of VMD; there is much mixing of the data, indicating that lift is not strongly dependent on volume mean droplet diameter, and more dependent on other parameters such as liquid water content, which may have a greater influence on the weight of the accreted ice in normal icing encounters (excluding freezing rain). For increasing LWC, lift exhibits a more defined decrease, as seen in Figures 10 and 11, however even this decrease of LWC is only on the order of 3 to 5% from LWC=0.35 gm/m^3 to LWC=0.75 gm/m^3. In Figure 12, C_L/σ clearly increases over a temperature range of -12.3 °F to +27.4 °F. For the same change in θ as in the case for torque, lift is not so clearly influenced; i.e., data overlap continually as C_L/σ decreases over icing time as seen in Figure 13.

Thrust

C_T/σ exhibits the same trends as C_L/σ, as expected, as lift and thrust are identical in nature for this case. Had forward motion of the aircraft been simulated then the values of lift and thrust would not have coincided, as a component of the total thrust affected by the ice accretion would have been delegated to forward motion only. Numerical differences between the two coefficients tend to enter in only the third or fourth decimal place. Figures 14 through 17 show C_T/σ as a function of icing time for the parameters of VMD, LWC, and θ. See Appendix A for statistical data concerning plots of C_T/σ and C_L/σ.

Concluding Remarks

Examination of the correlated data has provided encouraging results. The data show the effects of liquid water content, volume mean droplet diameter, temperature, and shaft angle. Qualitative trends correctly follow those known to exist in flight. The model exhibits the correct physical trends for an actual icing encounter, including reactions to shedding and post-cloud behavior. Multiple runs with the same parameter values, though not plotted formally here, have shown good repeatability. Torque rises as a function of icing time for all parameters tested, while lift and thrust decrease. It appears that this data, and the method from which it was provided, will prove helpful in future research and development of model testing in the area of data acquisition for all-weather flight certification.

References

1. U.S. Department of Transportation, Federal Aviation Administration, "Certification of Small Airplanes for Flight in Icing Condition," AC23.1419-1, September, 1986.
2. Flemming, R. and Saccullo, A., "Testof a Model Rotor in the NASA Lewis Research Center Icing Research Tunnel." NASA CR.
3. Guffond, D.D., "Icing and De-icing Test on a 1/4 Scale Rotor in the ONERA Wind Tunnel," AIAA Paper 86-0480, January 1986.
4. Miller and T.L., Bond, T.H., "Icing Reseach Tunnel Test of a Model Helicopter Rotor," NASA Technical Memorandum 101978, May 1989.
5. Bond, T.H., Flemming, R.J., and Britton, R.K., "Icing Tests of a Model Main Rotor," American Helicopter Society, 46th Annual Forum, Washington, D.C., May 1990.

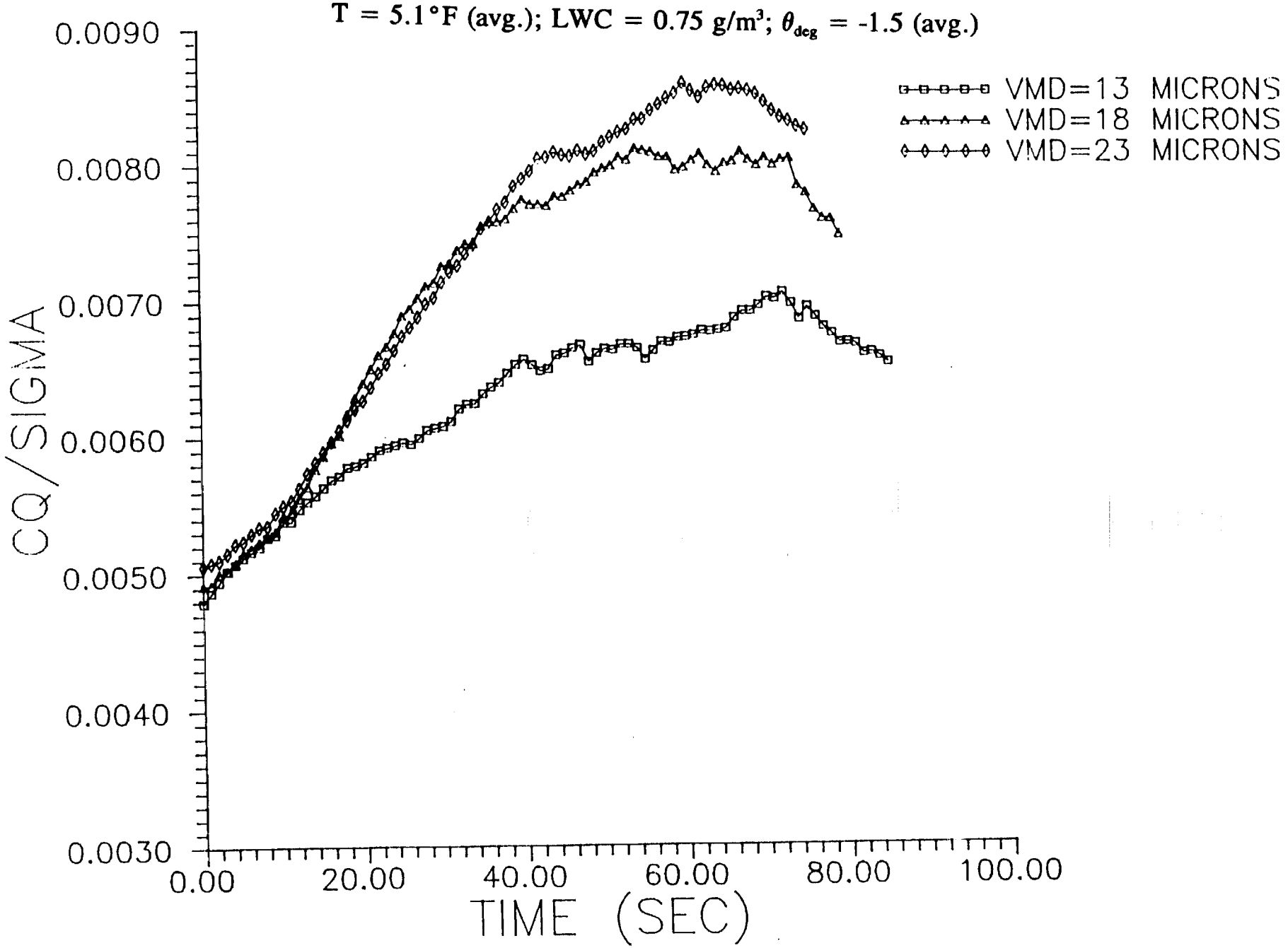

Figure 1. Torque as a Function of Icing Time

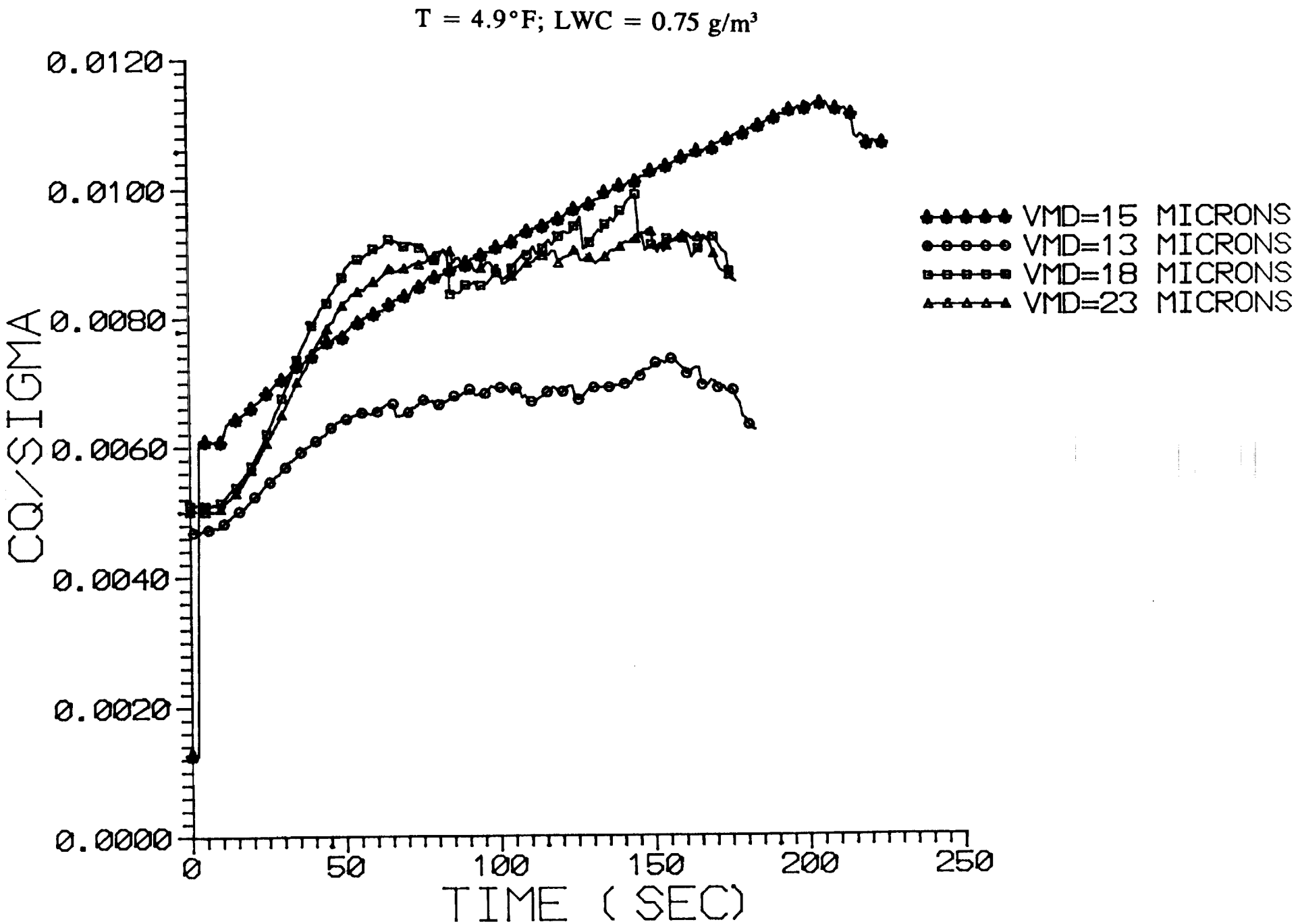

Figure 2. Torque as a Function of Icing Time

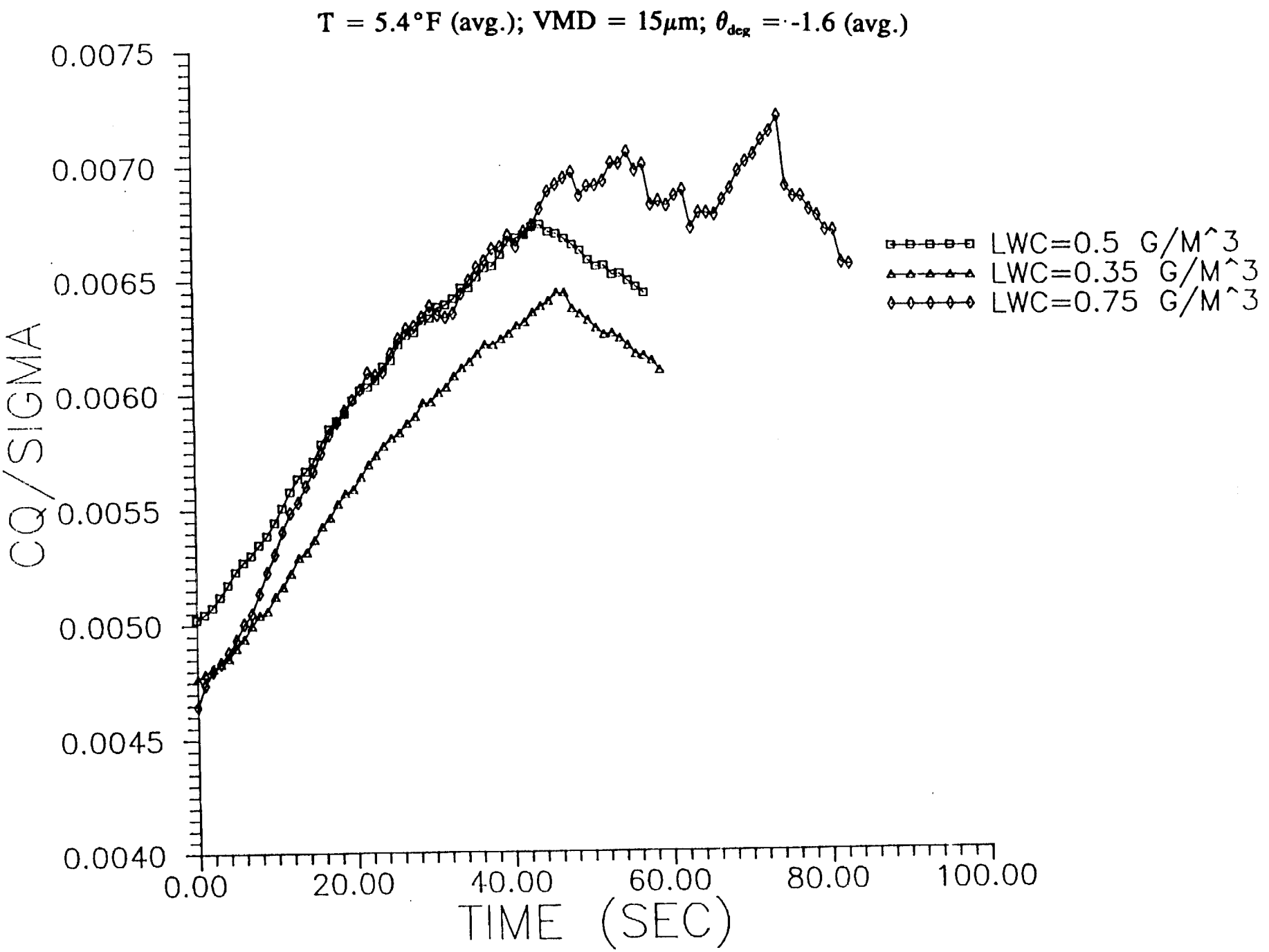

Figure 3. Torque as a Function of Icing Time

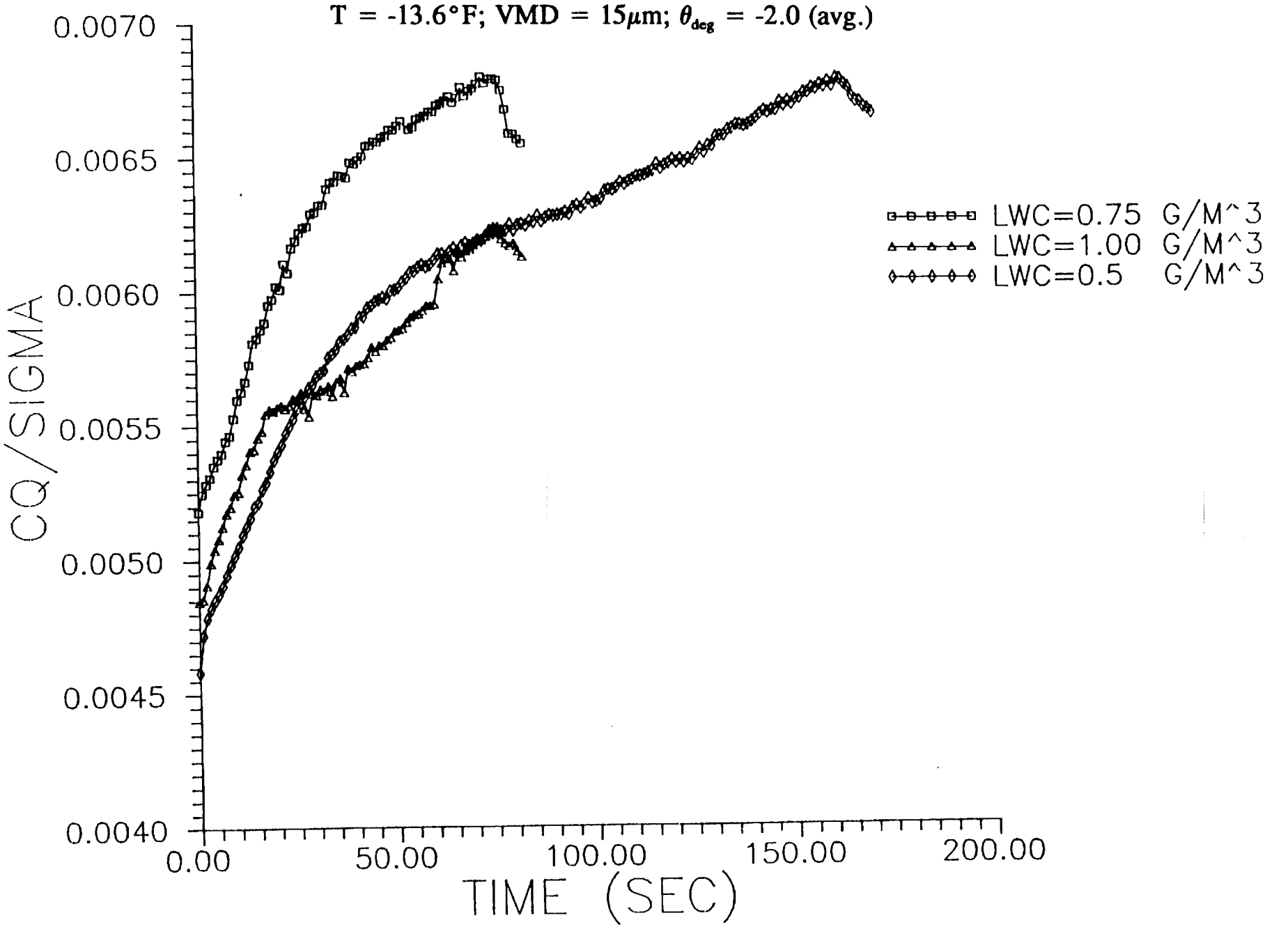

Figure 4. Torque as a Function of Icing Time

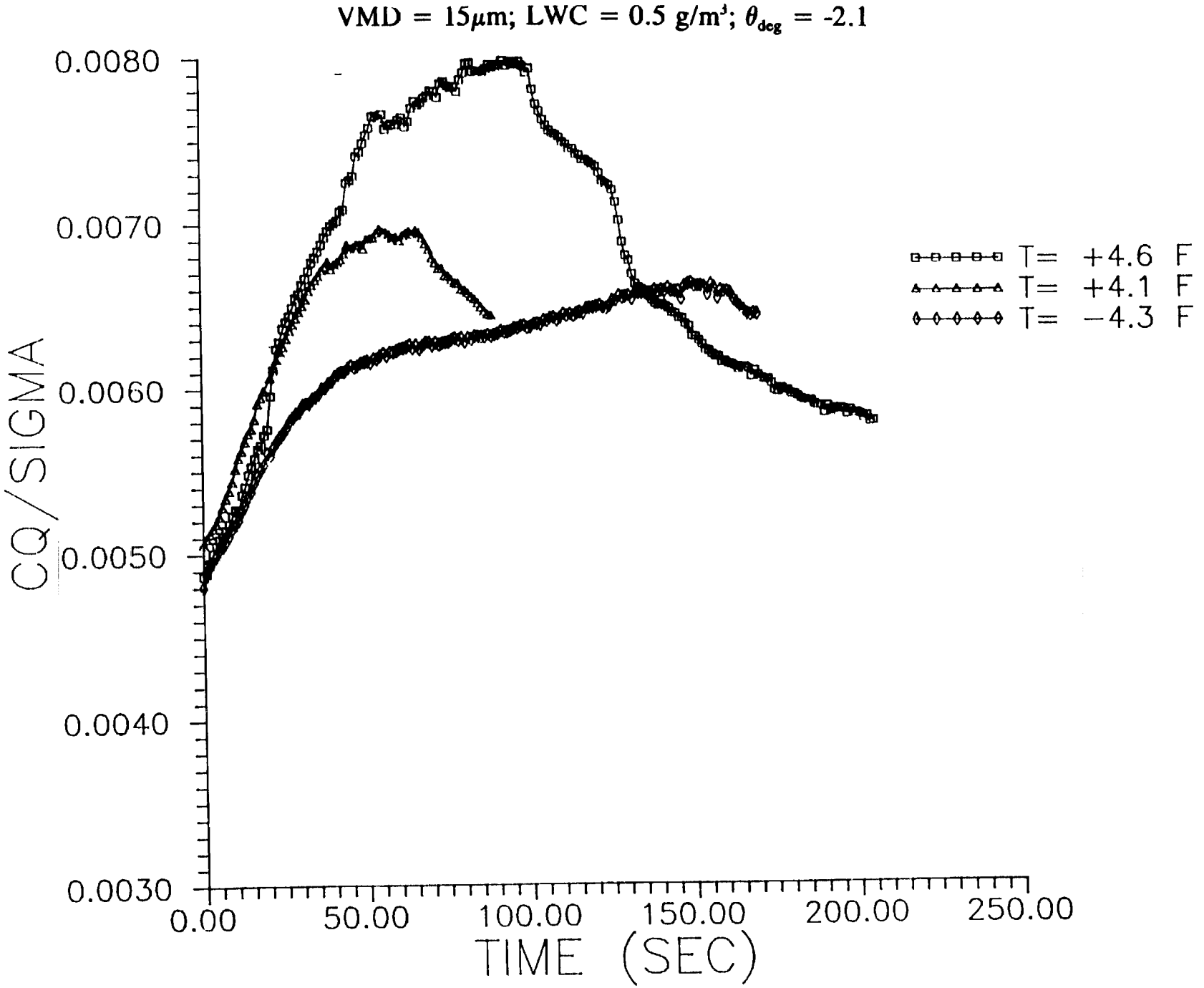

Figure 5. Torque as a Function of Icing Time

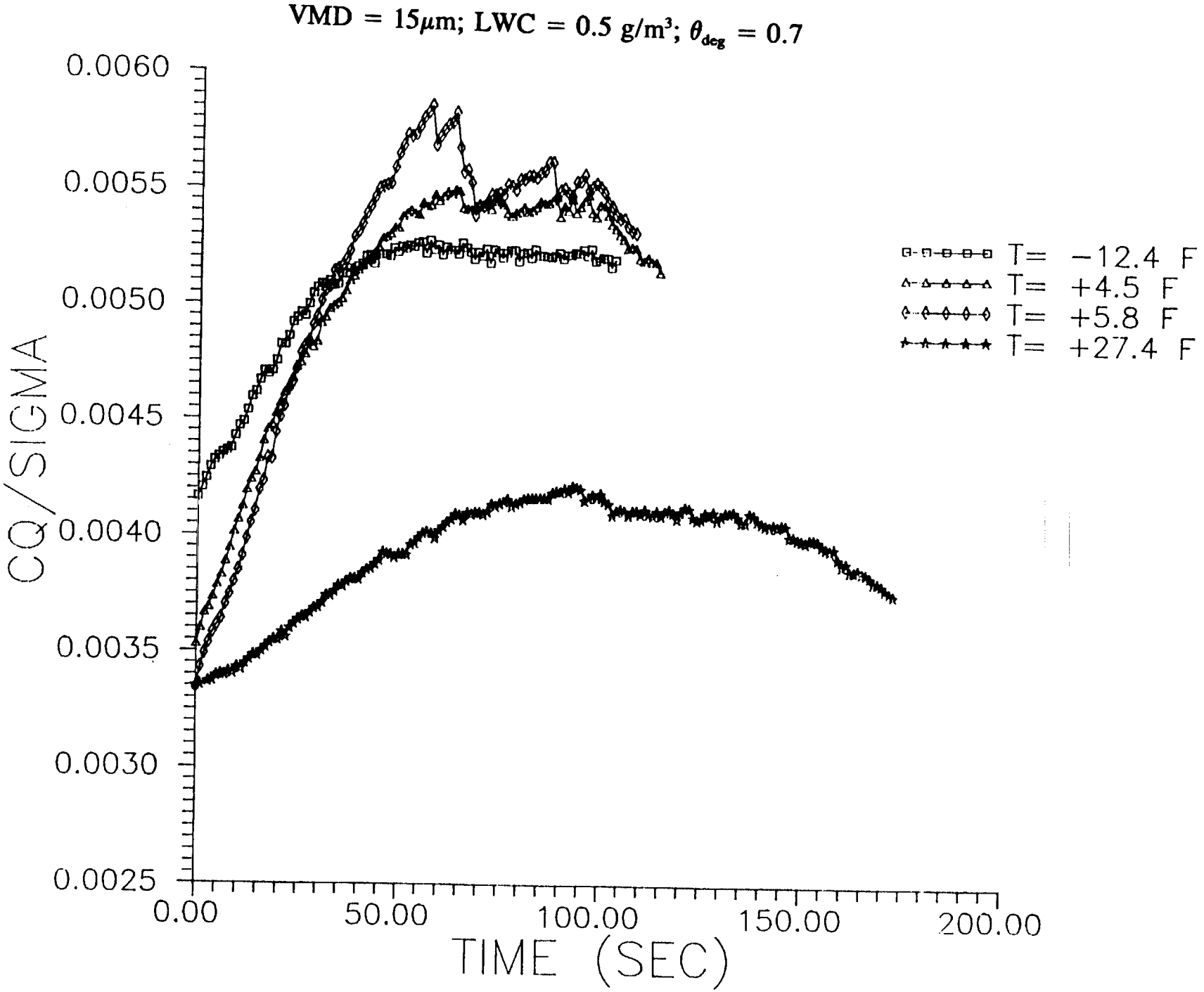

Figure 6. Torque as a Function of Icing Time

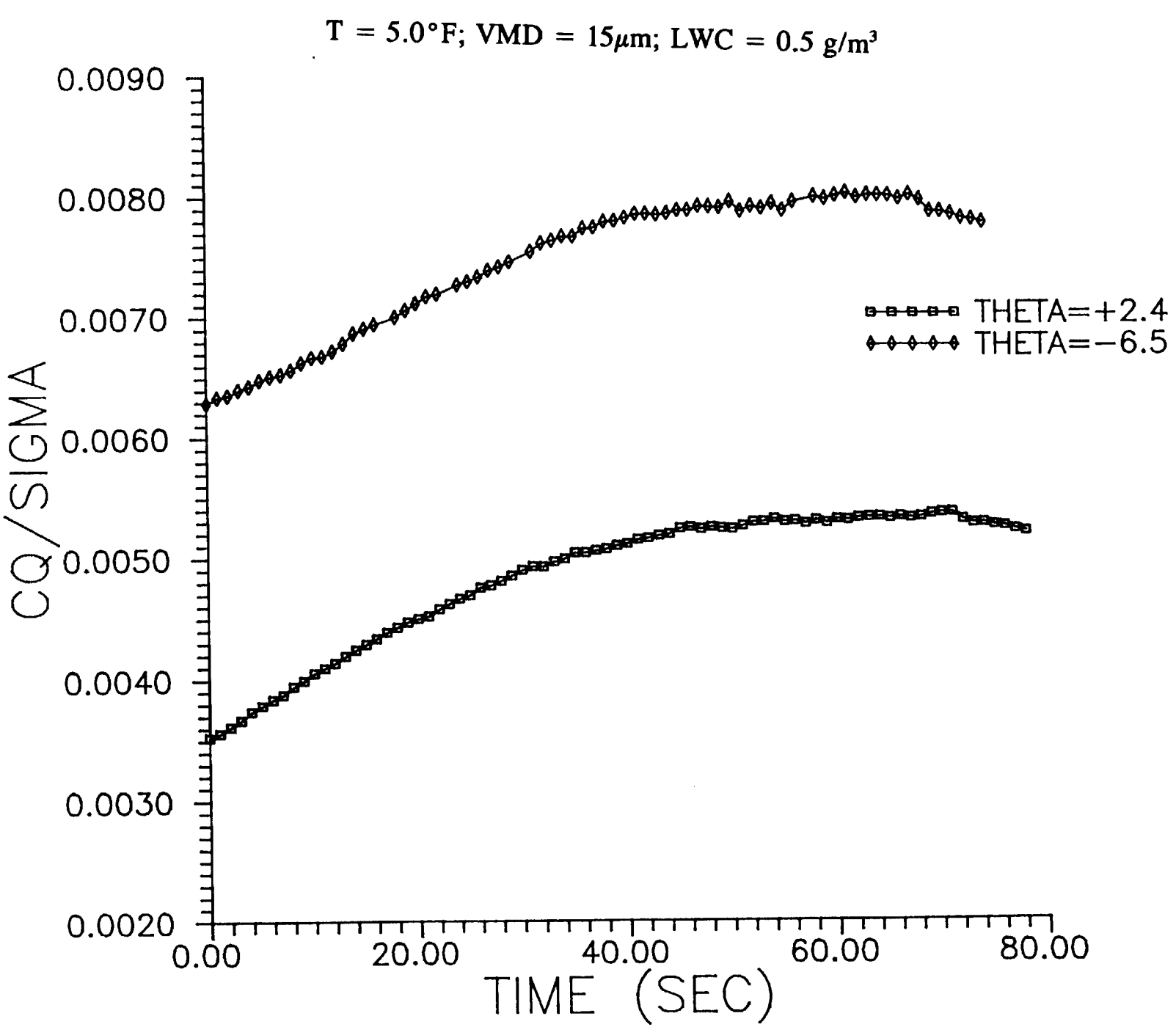

Figure 7. Torque as a Function of Icing Time

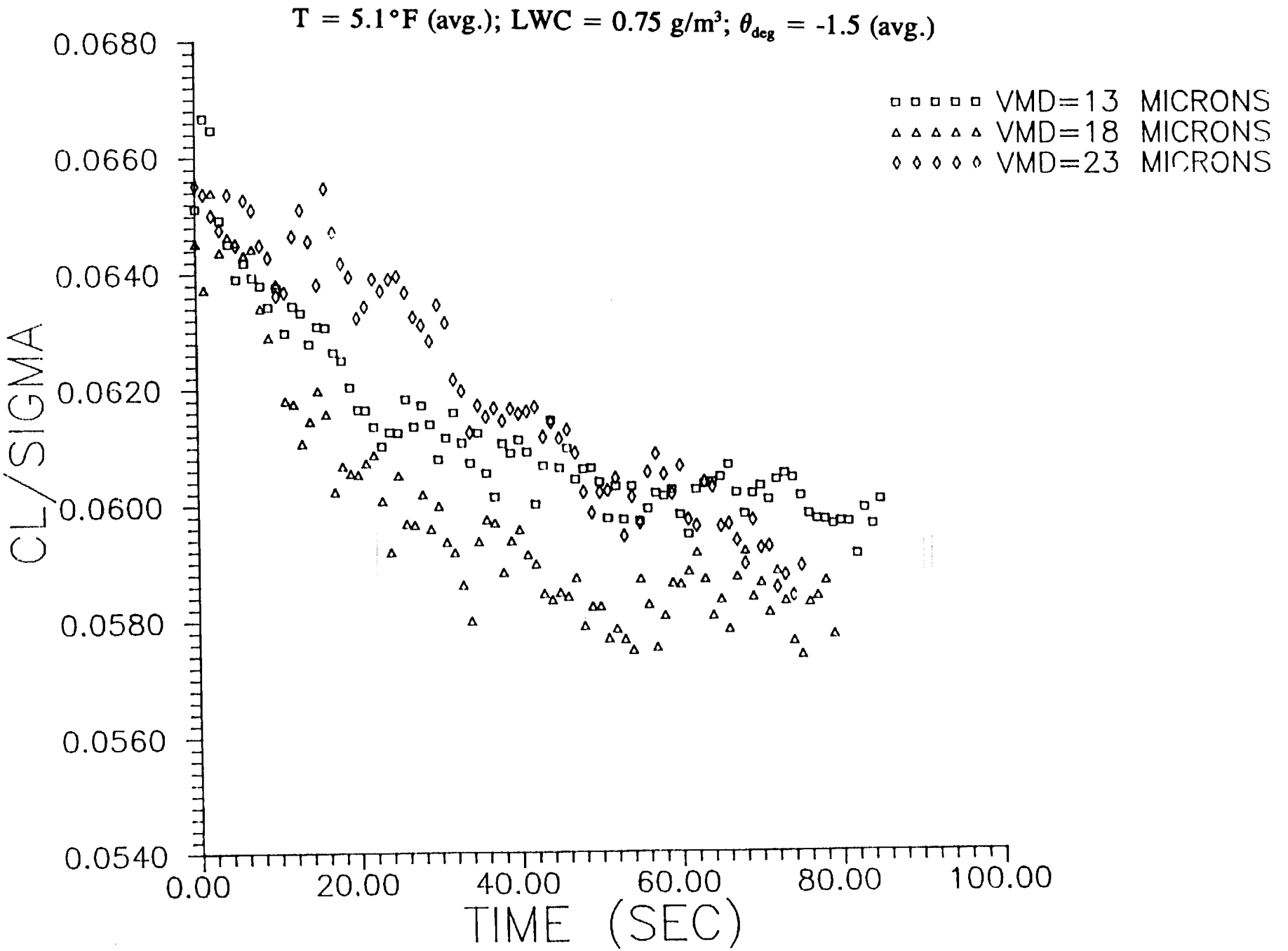

Figure 8. Lift as a Function of Icing time

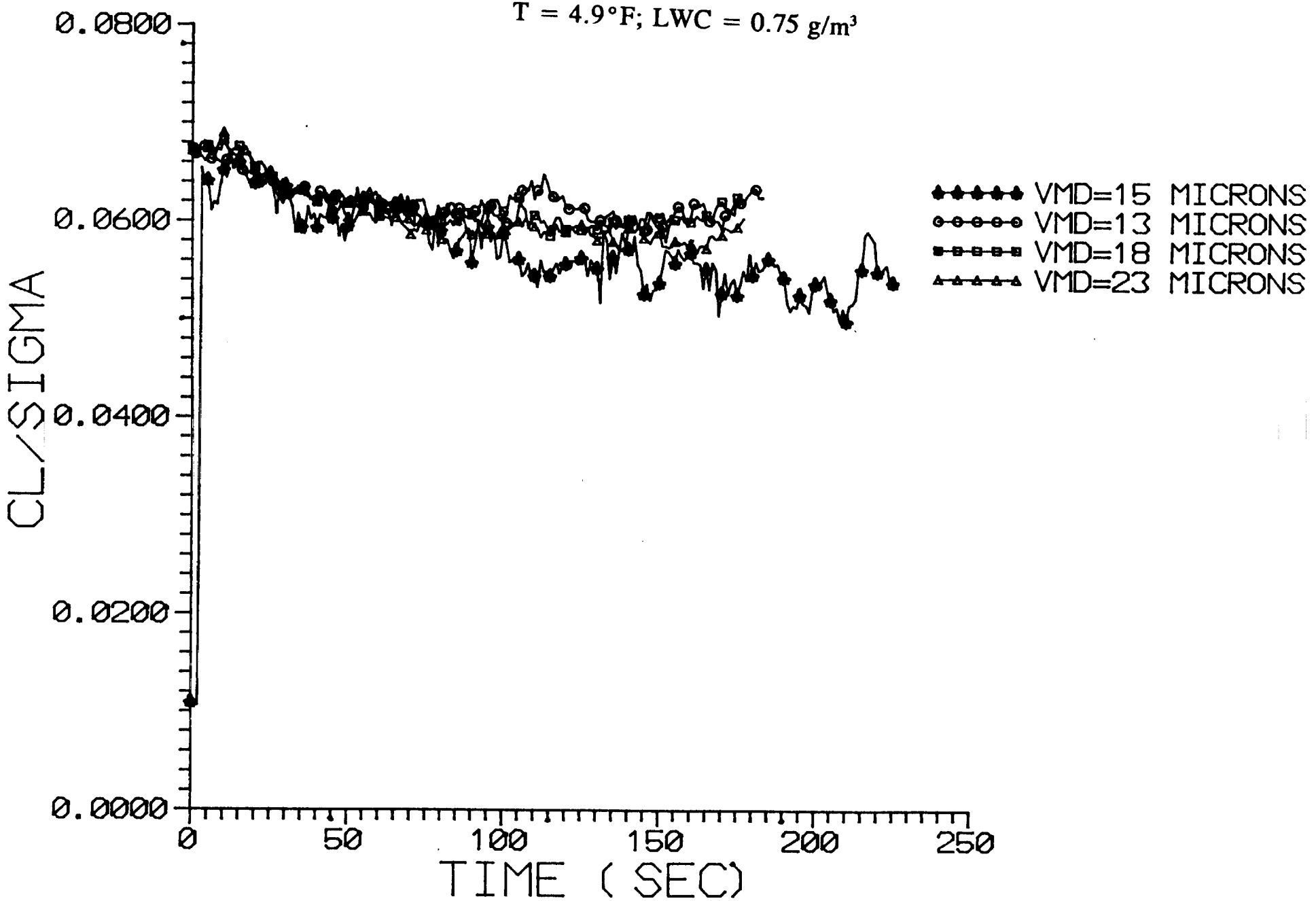

Figure 9. Lift as a Function of Icing time

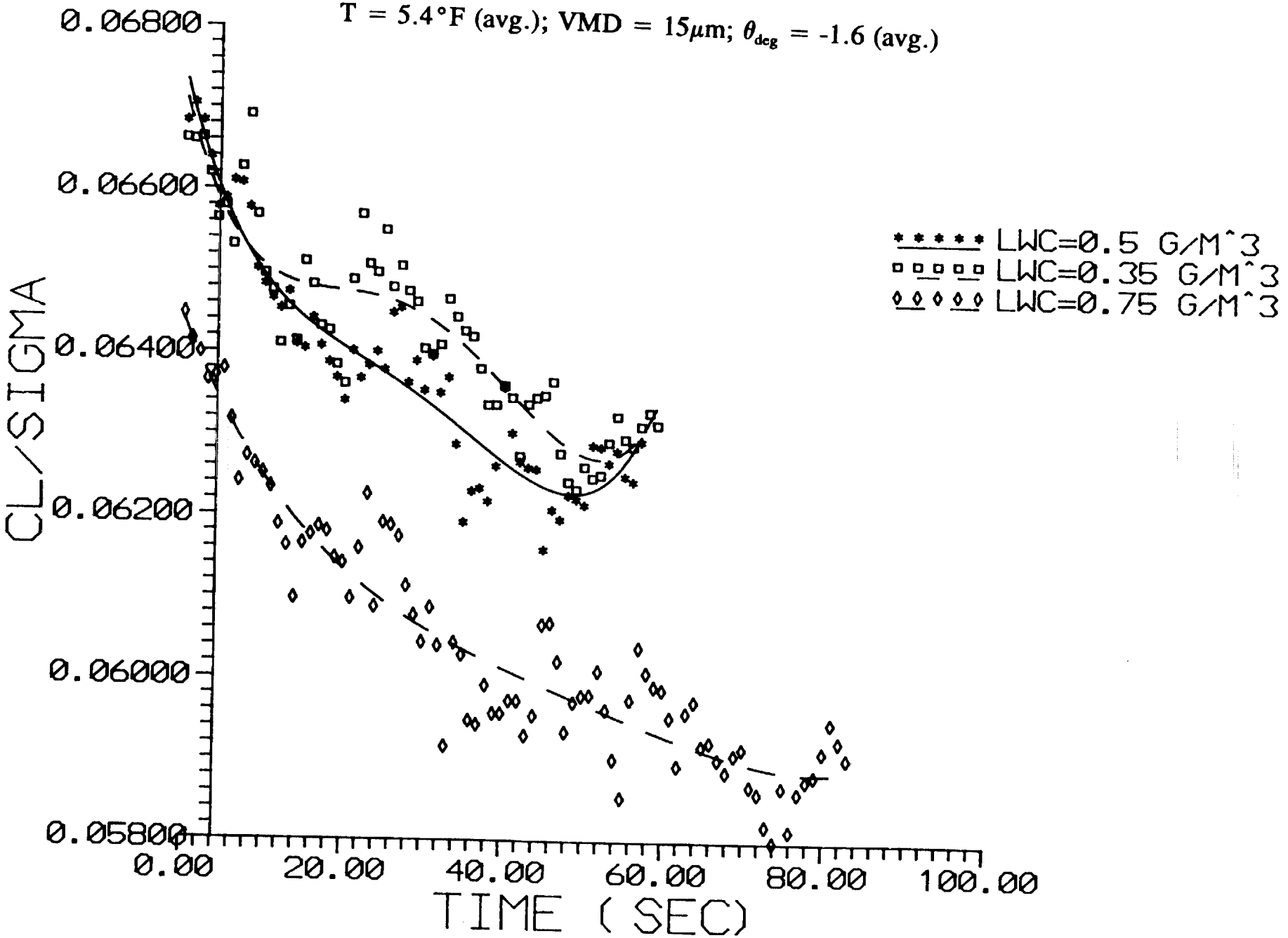

Figure 10. Lift as a Function of Icing time

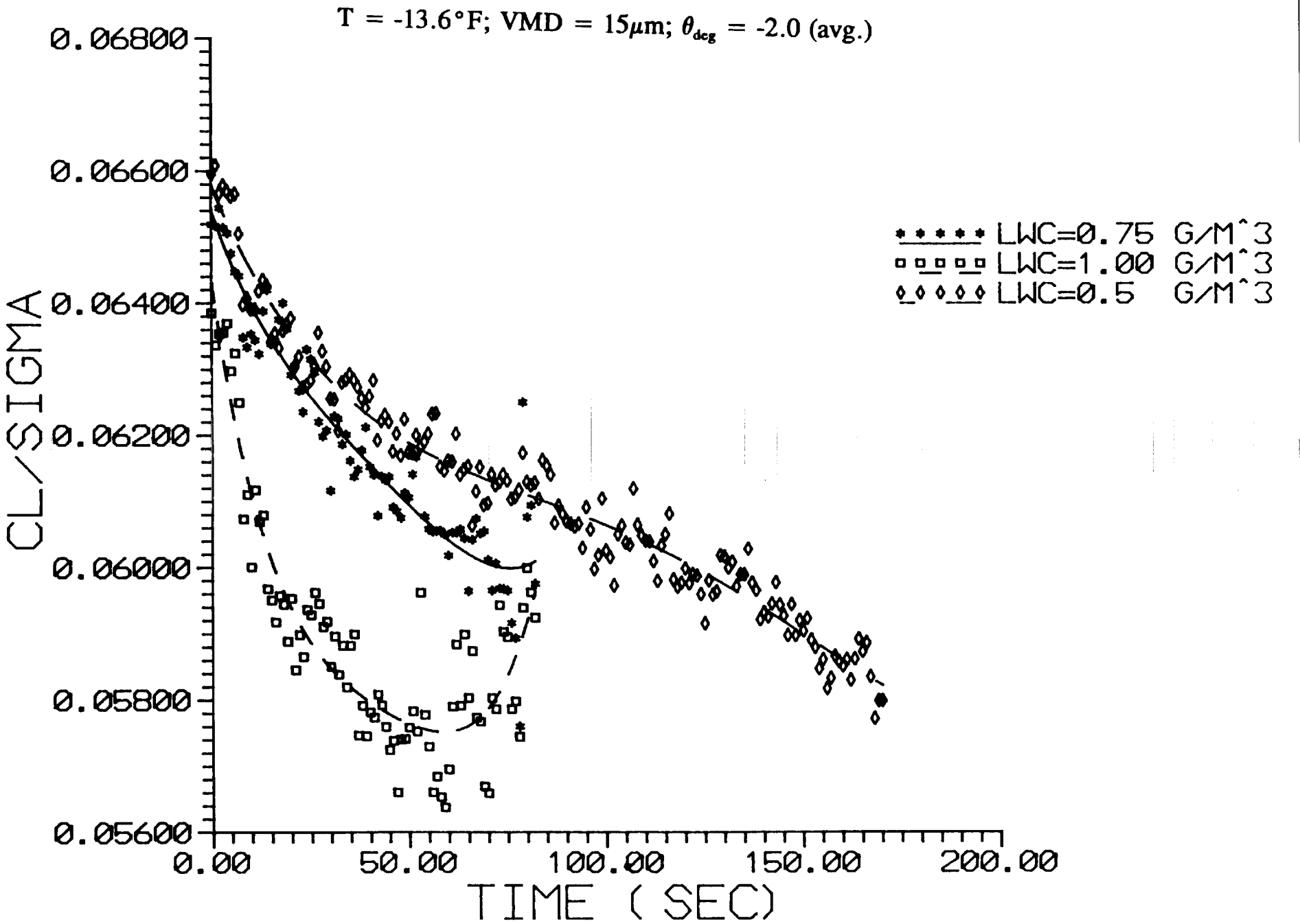

Figure 11. Lift as a Function of Icing time

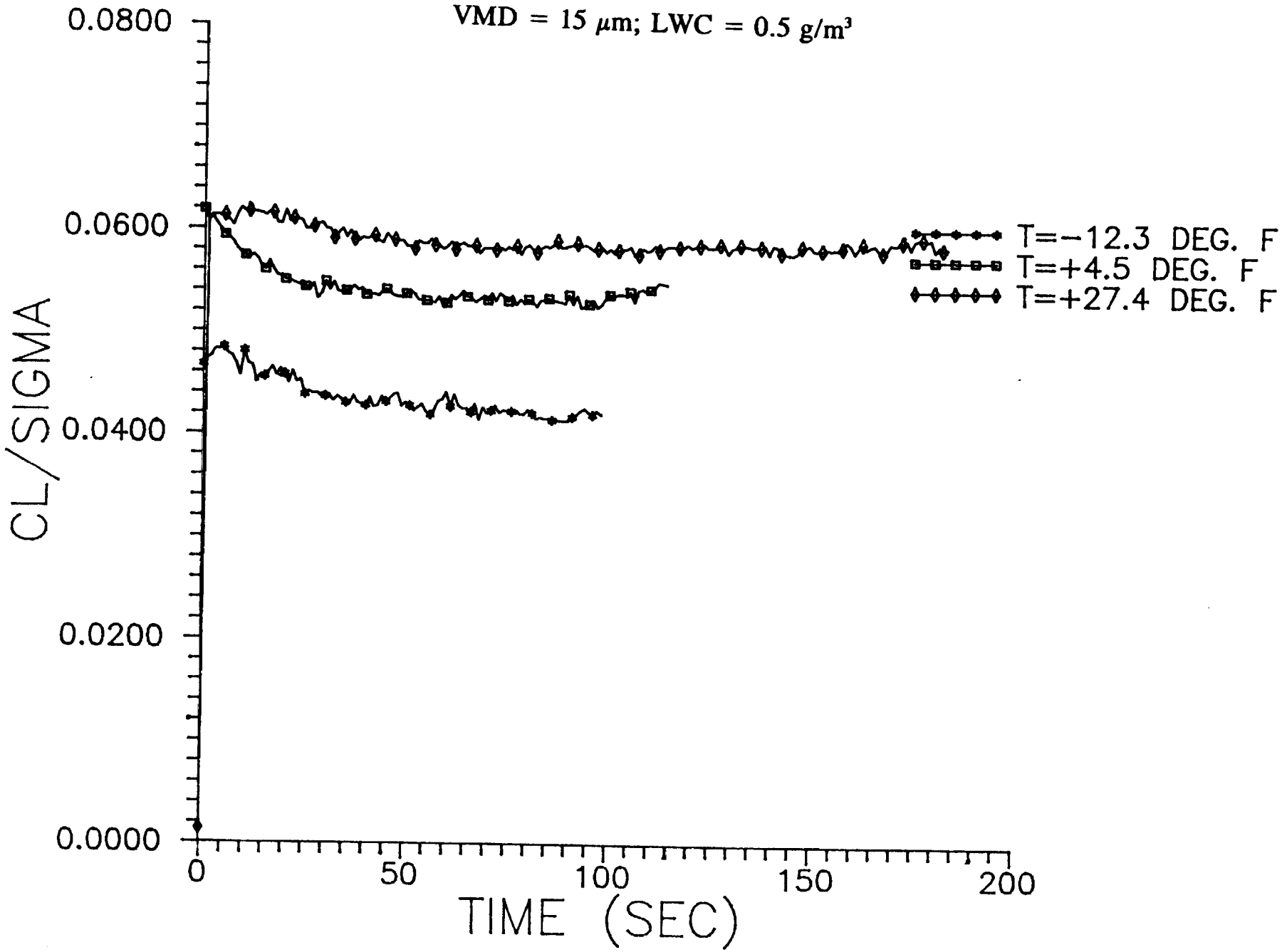

Figure 12. Lift as a Function of Icing time

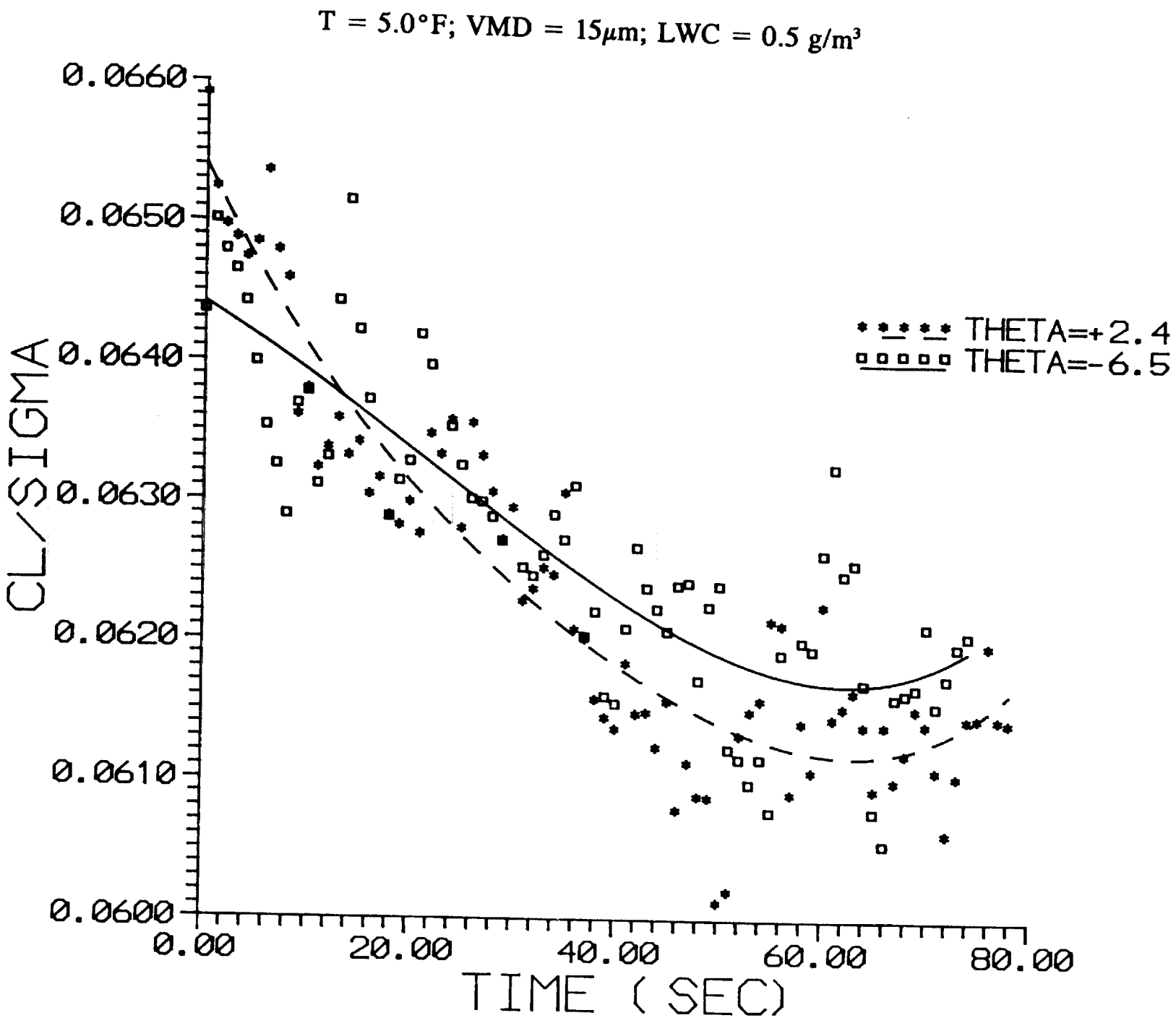

Figure 13. Lift as a Function of Icing time

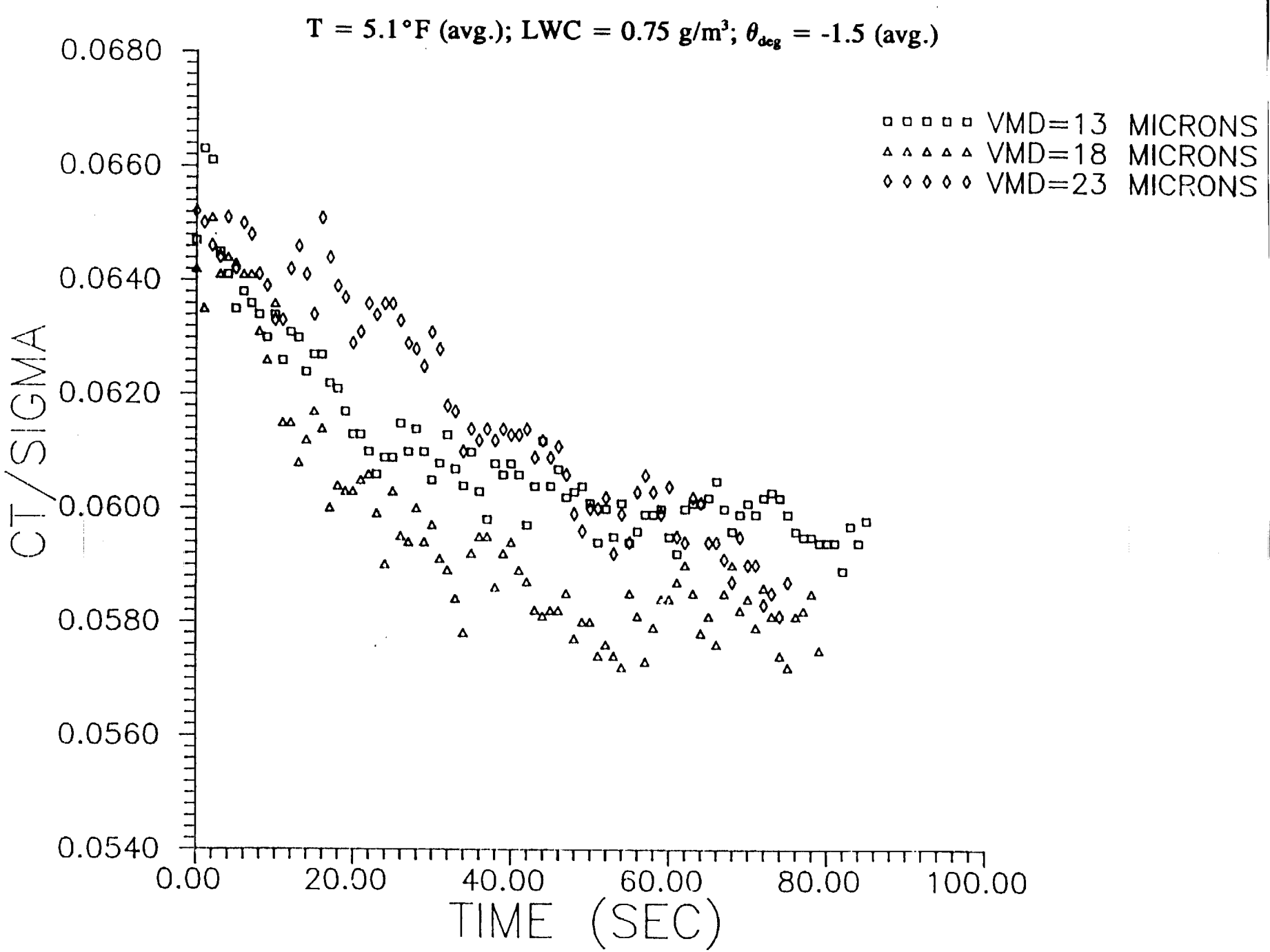

Figure 14. Thrust as a Function of Icing Time

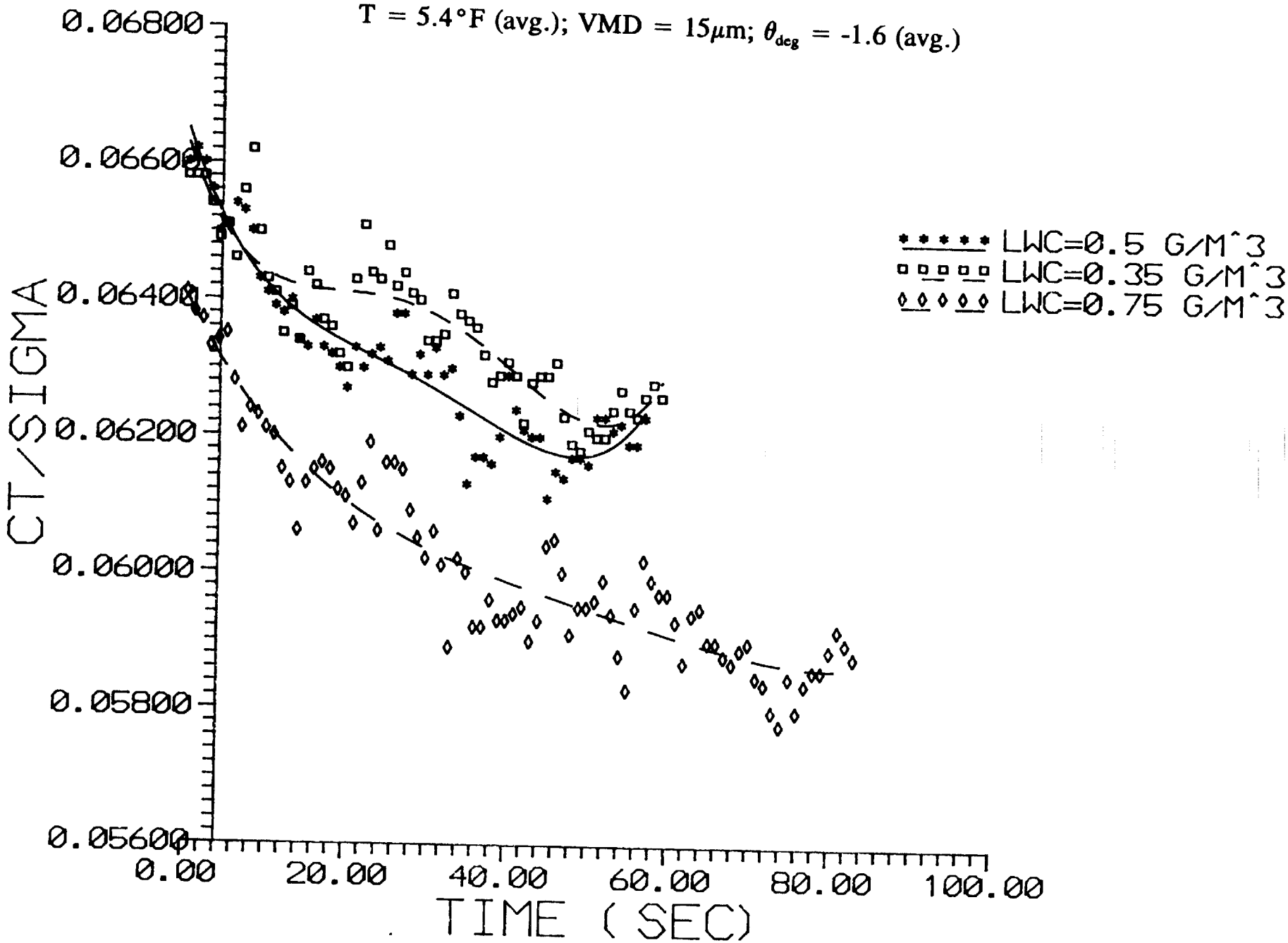

Figure 15. Thrust as a Function of Icing Time

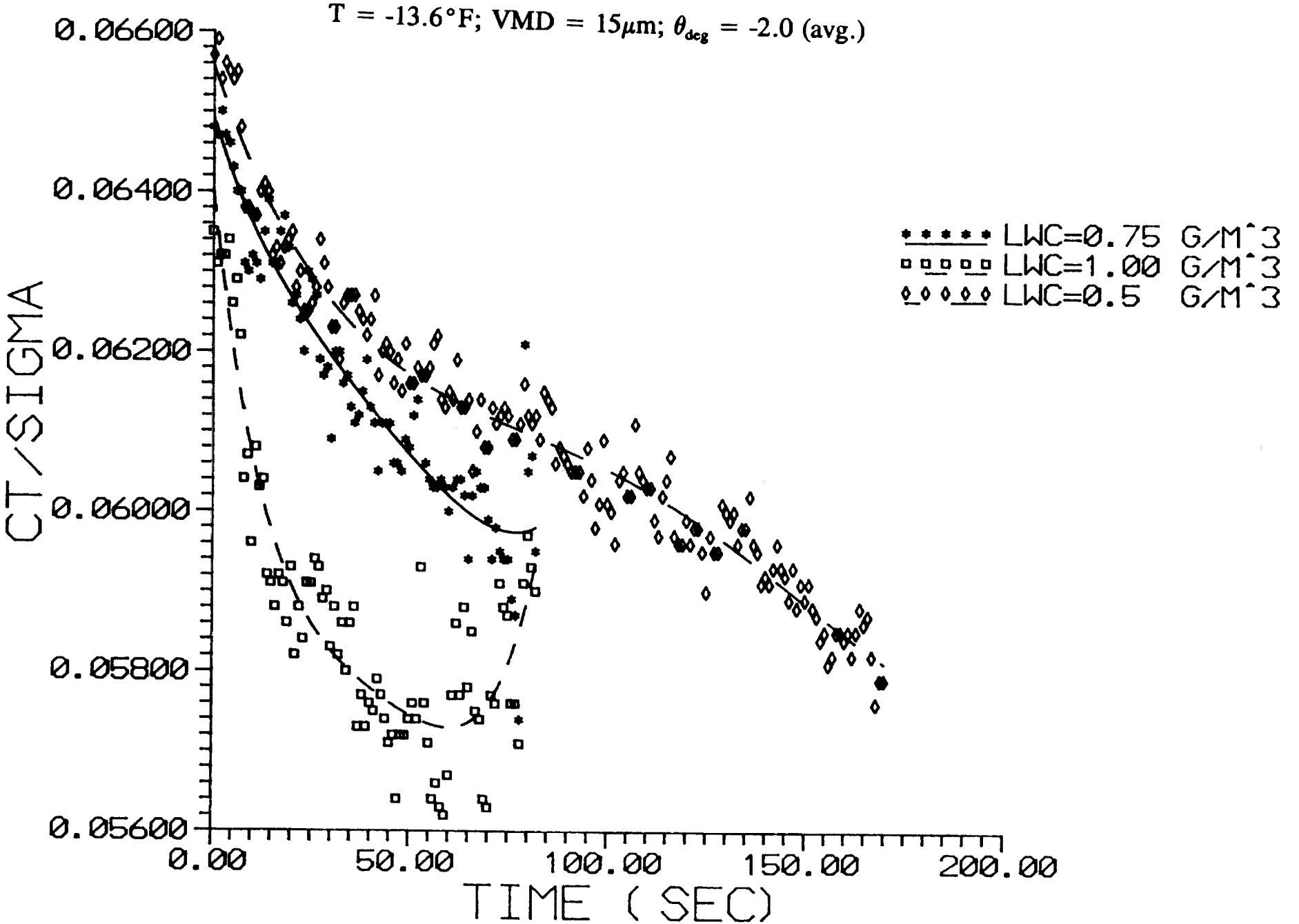

Figure 16. Thrust as a Function of Icing Time

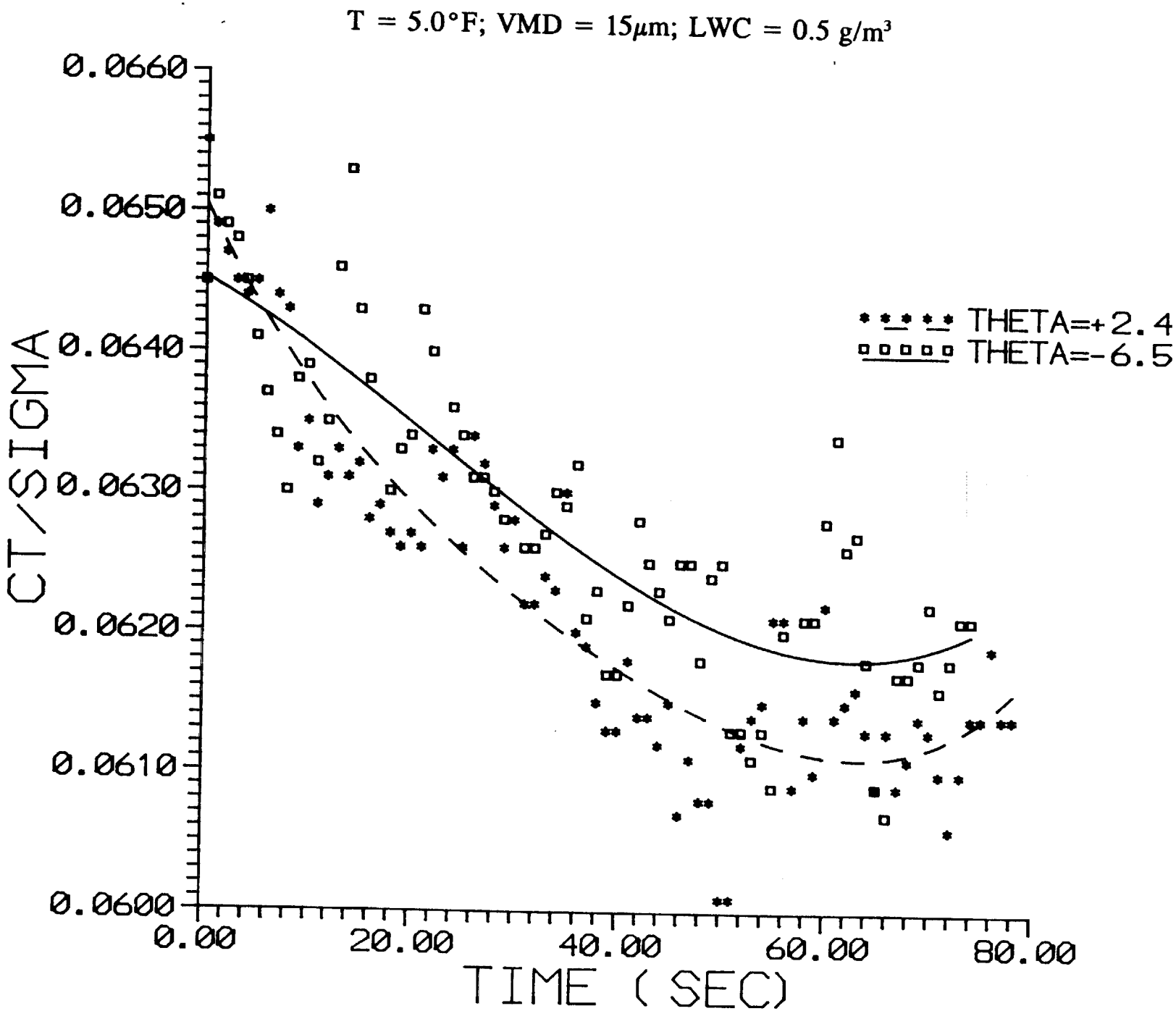

Figure 17. Thrust as a Function of Icing Time

Appendix A
Scatter Plot Statistics

RUN	C_L/σ		C_T/σ	
No.	AVG.	ST. DEV.	AVG.	ST. DEV.
70	0.06375	1.36E-3	0.0631	1.299E-3
72	0.06394	1.424E-3	0.0636	1.109E-3
75	0.06045	1.552E-3	0.0604	1.751E-3
85	0.06190	2.007E-3	0.0619	2.158E-3
87	0.06238	1.313E-3	0.0624	1.33E-3
89	0.06267	1.064E-3	0.0628	1.077E-3
90	0.06178	1.638E-3	0.0617	1.671E-3
91	0.06135	2.025E-3	0.0615	2.238E-3
99	0.06182	1.674E-3	0.0618	1.897E-3
100	0.05894	1.800E-3	0.0590	2.103E-3
101	0.06116	1.843E-3	0.0611	1.987E-3

The above statistics corespond to the data in those plots for which a large spread in values appeared, making trends more difficult to read directly. Only those runs and figures noted here are represented above: Runs 70, 72, and 75 correspond to Figures 3, 10, and 15; runs 85, 90, and 91 correspond to Figures 1, 8, and 14; runs 99, 100, and 101 correspond to Figures 1, 8, and 14; run 87 and 89 correspond to Figures 7, 13, and 17.

Appendix B

Bond, T. H., Flemming, R.J., and Britton, R. K., "Icing Tests of a Model Main Rotor," American Helicopter Society, 46th Annual Forum, Washington, D.C, May 1990.

ICING TESTS OF A MODEL MAIN ROTOR

Thomas H. Bond
National Aeronautics and Space Administration
Lewis Research Center
Cleveland, Ohio 44135

Robert J. Flemming
Sikorsky Aircraft Division, UTC
Stratford Connecticut

Randall K. Britton
Sverdrup Technology, Inc.
NASA Lewis Research Center Group
Cleveland, Ohio

ABSTRACT

A consortium composed of NASA, Texas A&M University, Bell Helicopter Textron, Boeing Helicopters, McDonnell Douglas Helicopters, and Sikorsky Aircraft conducted an experimental program to investigate the characteristics of a model rotor under icing conditions. This project resulted in the first U.S. test of a heavily instrumented model rotor conducted in the controlled environment of a refrigerated wind tunnel, the NASA Lewis Icing Research Tunnel. The tunnel entry used a Powered Force Model with a 1.83-m (6.00-ft)-diameter main rotor, with 0.124-m (4.9-in.)-chord main rotor blades fabricated specially for this experiment. Test conditions included a range of liquid water content and median volume droplet diameters that fell within the FAA and DOD icing envelopes. The test data show the effects of icing on rotor lift, rotor torque, blade loads, and vibration. Ice shapes and ice dimensions were taken, and molds were made of three ice shapes. High-speed movies were taken to document ice shedding. The results have been compared with analytical accretion predictions.

NOTATION

A_c	accumulation parameter
B	total pressure, kN/m^2
C_L/σ	lift coefficient/solidity
C_m	model chord, m
C_F	full scale chord, m
C_Q/σ	torque coefficient/solidity
C_T/σ	thrust coefficient/solidity
c	chord, m
d	droplet diameter, μm
K_o	modified inertia parameter
LWC	liquid water content, g/m^3
R	leading edge radius, m
T	static air temperature, °C
V	free stream velocity, m/sec
X	propulsive force
σ	solidity (0.173)
μ	advance ratio
ρ	ice density, g/m^3
τ	icing time, sec
ΩR	rotor tip speed

INTRODUCTION

The majority of U.S. military and civil helicopters have a restricted or no clearance for operating in forecast icing conditions. This is due in part to the lack of adequate rotor deicing systems, extreme rotor sensitivity to ice accretion, and the expense of system qualification for the full icing envelope. Procedures have been established to use icing tankers and/or ground icing facilities, but these approaches have not adequately simulated natural icing conditions. Because of the trend toward design of all-weather rotorcraft, it is necessary to develop and validate the experimental techniques to understand the effects of ice on rotor performance and to determine the design requirements for rotor ice protection. Analytical methods are now being developed to predict rotor performance in icing, including ice accretion and ice shedding. The use of a model rotor to provide a less expensive and more repeatable source of test data will aid in the validation of these analytical methods and support the overall goal toward more expedient certification procedures (Figure 1). The French undertook a model icing program where a 1/4-scale model rotor was tested in the ONERA SIMA wind tunnel at Modane, France (Reference 1). This testing showed that a model program had promise, but the data acquired were too limited to provide a correlation base. However, this testing prompted the interest of rotorcraft icing researchers in the United States. A rotor icing consortium evolved to identify and pursue an approach to model rotor testing in an icing environment. NASA Lewis Research Center undertook a program with university and industry participants to demonstrate the usefulness of the model rotor test technique as an approach for obtaining meaningful icing data for rotating systems.

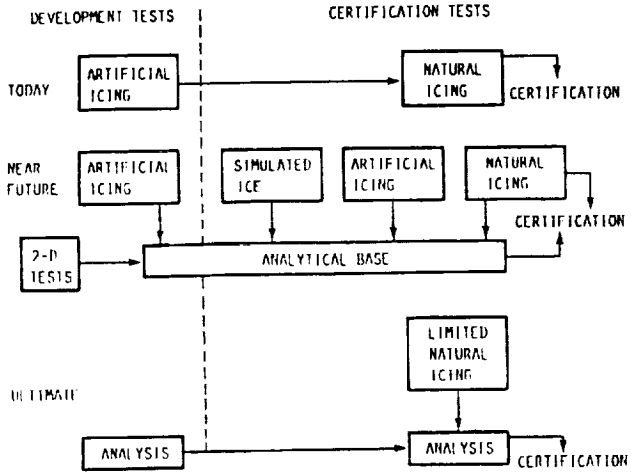

FIGURE 1. - CERTIFICATION FLOW DIAGRAM FOR ROTORCRAFT ICING.

TECHNICAL APPROACH

The Rotor Icing Consortium is composed of members from the four major helicopter companies: Bell Helicopter Textron, Boeing Helicopters, McDonnell Douglas Helicopters, and Sikorsky Aircraft Division of United Technologies, plus representatives from NASA Lewis Research Center (LeRC), U.S. Army Aviation Research and Technology Activity-AVSCOM, and Texas A&M University. The consortium worked during the early part of the program to identify the necessary tasks and the means to achieve them. Each of the members was given specific responsibilities, as outlined in Table 1.

A two model approach was selected as the most effective means to accomplish the program goals. A lightly instrumented OH-58 tail rotor (Figure 2) that had been modified to approximately operate as a main rotor was chosen as the initial test article. This would be followed by the more sophisticated Sikorsky Basic Model Test Rig (BMTR) Powered Force Model (PFM) (Figure 3) to provide detailed rotor performance measurements. The OH-58 IRT entry would establish operational techniques for the more complex model, define tunnel test capabilities for a rotorcraft entry, and gather preliminary data. The OH-58 model test was completed in October 1988 and the results presented at the 1989 American Helicopter Society Annual Forum (Reference 2). The conclusion of this initial test indicated the tunnel was capable of being used for model rotor icing. The test techniques developed for the OH-58 entry were refined to provide a greater probability of success for the PFM entry.

The initial PFM Icing Research Tunnel (IRT) entry was scheduled for an 8 week period during July to September, 1989. During this time the model was installed and icing testing began. However, blade tracking problems and the high humidity, warm ambient conditions precluded testing at very cold temperatures. A total of 44 icing encounters occurred in the 14 days of testing.

At the end of this initial test period, the model was removed and a second entry scheduled for November 1989. Between tests, the model was serviced, data reviewed, high speed motion picture capability added, and methods for improving blade track were prepared. This second entry resulted in 41 icing encounters in 8 test days.

MODEL AND FACILITY DESCRIPTIONS

Icing Research Tunnel

The IRT is a closed-loop refrigerated wind tunnel. A 4100 hp fan provides airspeeds up to 134 m/sec (300 mph). The 21 000 ton capacity refrigeration heat exchanger can vary the total temperature from -1.1 to -42 °C (Figure 4). The spray nozzles provide droplet sizes from approximately 10 to 40 μm median volume diameter (MVD) with liquid water contents (LWC) ranging from 0.2 to 3.0 g/m^3. The tunnel is 1.8 m (6 ft) high and 2.7 m (9 ft) wide.

Armor plates were attached to the walls of the tunnel test section, during the model rotor test, to protect personnel in the control room. Video systems were installed to monitor the test area and local blade positions, and to provide tracking information. For several runs 0.635 mm (0.025 in.) aluminum sheets were placed on energy absorbing material and attached to the armor plating in line with the rotor disk plane. The shed ice made permanent dents in the sheets that will be calibrated to calculate the impact energy of the ice that struck them. A high speed 16 mm camera was used to capture ice shedding from the blades. The movies were taken at 2000 frames per second and capture approximately a 60° arc of the rotor rotational field.

Powered Force Model

The Sikorsky PFM is a self-contained, general purpose rotor test rig. The load measuring systems, rotor power, and control mechanisms are located within the model frame. The PFM can accept a wide range of rotor systems and fuselage skins. The rig is capable of accepting a fuselage and powered tail rotor, each containing its own balance system. For this project only the main rotor and its balance were installed. The attachment of power, lubrication, control and signal lines complete the model installation. The main rotor was located 1.02 m (3.35 ft) above the tunnel floor, about 0.10 m (0.33 ft) above the centerline. The U.S. Army UH-60A model skins were used to enclose the balance and rotor hardware (Figure 3). A small rotor head fairing contained the hub accelerometers. While the fuselage skins are scaled for a 2.86 m (9.37 ft) rotor, tunnel dimensions dictated the use of a 1.83 m (6.00 ft) rotor for this test.

The rotor head used for this project (Figure 5) was a Sikorsky-designed and NASA Langley-owned general purpose, four bladed, fully articulated head with coincident flap and lag hinges at the 8.3 percent (76 mm or 3.00 in.) radial station. The hub has adjustable lead-lag

TABLE 1. - ROTOR ICING CONSORTIUM RESPONSIBILITIES FOR MODEL ROTOR ICING TEST

Company	Tasks
NASA Lewis	Project coordination; icing test techniques development for model rotor icing test
Propulsion Directorate-AVSCOM	Icing tunnel test hardware
Bell helicopter	PC-based safety of flight system
Boeing helicopters	Test plan; analytical modeling
McDonnel Douglas helicopters	Composite rotor blade design and construction; test support
Sikorsky Aircraft	Powered force model and associated hardware; data acquistion and reduction; test support
Texas A&M University	PC-based data acquisition and reduction system; test support

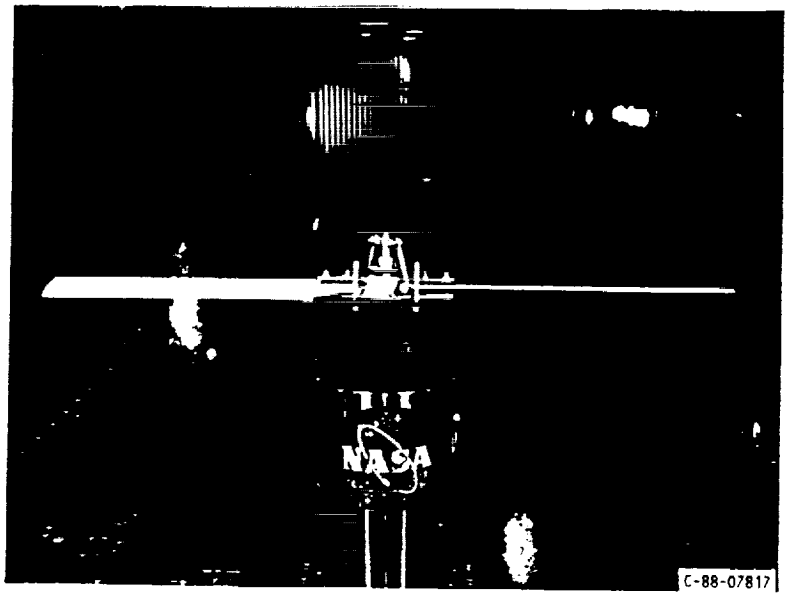

FIGURE 2. - OH-58 TAIL ROTOR ASSEMBLY.

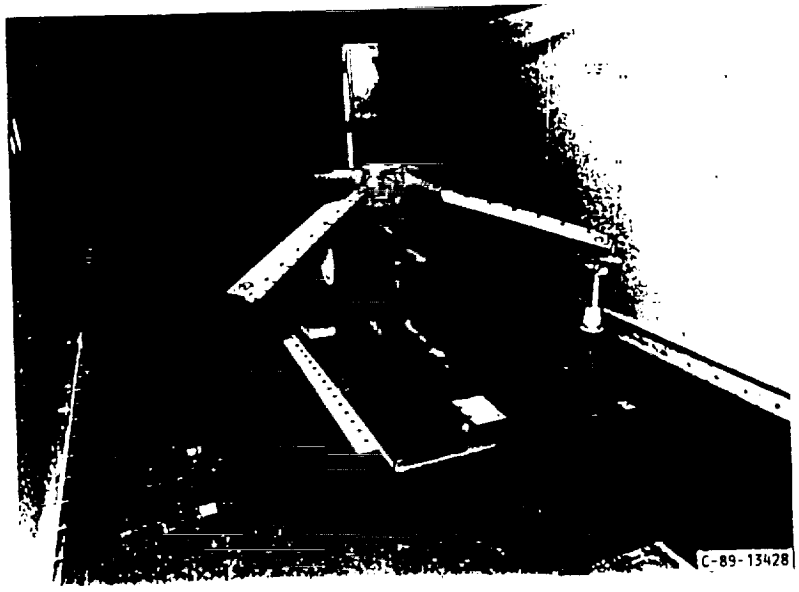

FIGURE 3. - MODEL MAIN ROTOR ASSEMBLY IN THE IRT.

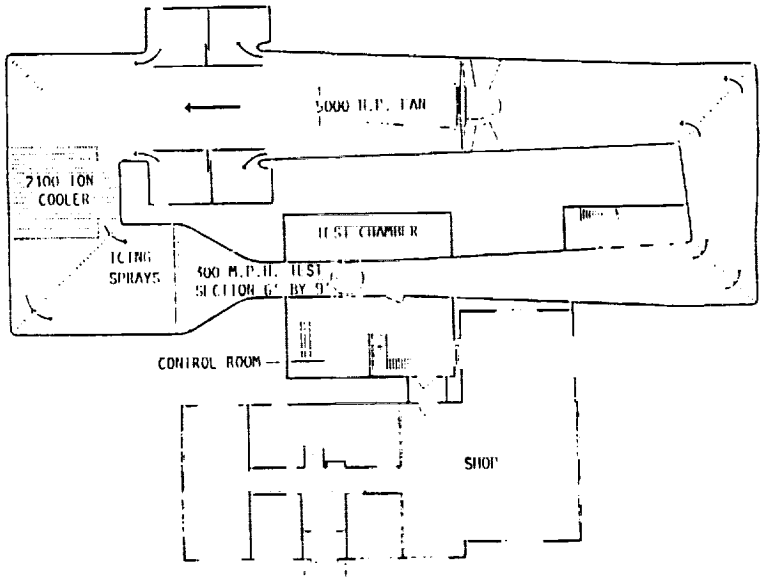

FIGURE 4. - NASA LEWIS ICING RESEARCH TUNNEL.

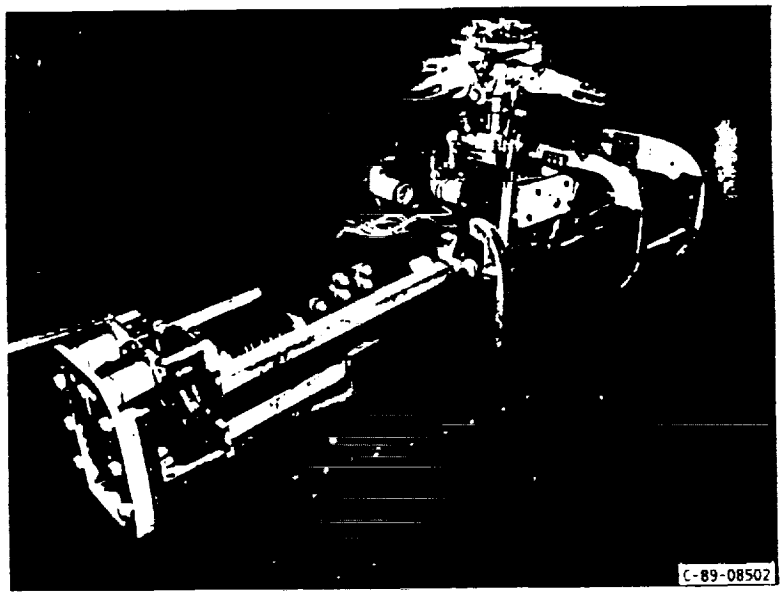

FIGURE 5. - SIKORSKY PFM ROTOR HEAD AND FORCE BALANCE ASSEMBLY.

dampers and for this test it had a zero pitch-flap coupling (δ_3). In order to preserve a consistent lead-lag damping coefficient during the variation in the IRT temperature, the rotor viscous dampers were electrically heated to maintain the fluid at about 10 °C. Potentiometers mounted on the flap, lead-lag, and pitch axes provide positional information for the rotor system relative to the shaft.

The PFM main rotor was driven by two Task 3-phase variable frequency induction electric motors. As installed, the motors can rotate at speeds up to 8000 rpm. A 3.5 to 1 reduction gear box operates the rotor shaft speed to a maximum of 2286 rpm, which equates to a rotor tip speed of 219 mps (718 fps). Each motor has a continuous rating of 60 hp. Rotor speed was measured using an optical encoder. Model power was supplied by a variable frequency motor-generator set provided by the Aeroflightdynamics Directorate, U.S. Army Aviation Research and Technology Activity. The motor-generator set featured a digital closed-loop rpm feedback control, which maintained a set rotor speed under the power variations that occurred due to ice accretion, shedding, and control changes.

Individual elements of the model are described in the following paragraphs.

Load measurement system. - The rotor forces and moments (except torque) were measured using a Modern Machine 367-301 strain gage balance. The balance was gimbal-mounted to the model frame with a soft spring attachment, which lessens the possibility of ground resonance. The balance was electrically heated to maintain it at the calibration temperature of 20 °C. Rotor torque was obtained by measuring the reaction force between the gearbox (which was mounted on bearings) and the gearbox frame with a Revere Model USPi-5-B load cell. A 102 channel slip-ring was used to transfer the rotating system signals from blade gages, pushrods, motion hardware, and accelerometers to the fixed system. It also provided power to the damper heaters.

Control system. - The swashplate control components consisted of rotating pushrods and scissors, the swashplate, three electromechanical actuators, and a stationary scissors. Control inputs were made at the control console with cyclic and collective joystick controllers. The input signals were electronically mixed by the controller which then moved the model actuators. A closed-loop feedback circuit monitored the actuator motion. Resolved shaft axis cyclic and flapping first harmonic coefficients were obtained from potentiometers located on the rotorhead. These values were displayed graphically and numerically to facilitate rotor trimming.

Shaft angle control. - Shaft angle for this test was set by the model operator using a remotely driven linear actuator located on the test rig support frame. A pitch arm transferred the linear motion of the actuator to the rotating motion of the model shaft. This resulted in both a translational and model pitch motion for the rotor. The model support shaft angle range was from -10 to +3°. The angles set by the shaft angle control were corrected by the gimbal deflection angle and aerodynamic wall corrections to obtain the true total shaft angle.

Main Rotor Blades

Ten blades were designed and built by the McDonnell Douglas Helicopter Company using molds built by Sikorsky Aircraft. The blades for the 1.83 m (6.00 ft) diameter rotor had NACA 0012 airfoils with a chord of 0.124 m (4.9 in.), a -10° linear twist, and a taper ratio of 1. The blade weight had to be kept to a minimum to stay within rotor head stress limits at the design rotor speed. The weight constraint resulted in

a thin walled hollow spar, an unsupported trailing edge, and unprotected airfoil surfaces. These design restrictions led to problems during cold temperature operations. The blades behaved differently, causing variations in tracking. It is believed that temperature cycling and the unfilled trailing edge area caused the tracking changes. Two of the blades were instrumented with strain gages in the flatwise, edgewise, and torsional axes to provide blade loading information for safety of flight. The data from the edgewise strain gages proved to be very useful in identifying shedding events. This prompted the addition of root edgewise strain gages to the noninstrumented blades prior to the second entry.

The rotor blades were marked on their upper surfaces with the blade number and spanwise decade percentage marks to provide identification of the blade being monitored and the relative location of the ice that was shed.

INSTRUMENTATION AND DATA SYSTEM

Test Parameters

The test parameters measured fell into two main categories - those that were of research interest and those that were required solely for safety-of-flight. The 41 parameters in the first category were processed by the Dynamic Data Aquisition System (DDAS) and saved on both digital tape and floppy disks. Derived parameters were also computed using the DDAS and saved for further analysis. The test parameters used for analysis include the following:

- Main rotor balance loads (6 components)
- Main rotor torque and speed
- Tunnel temperature, and static and total pressure
- Liquid water content (measured by Johnson-Williams probe)
- Control positions (4) and instrumented blade angles (3)
- Resolved blade flapping and coning (3)
- Instrumented blade flatwise (3), edgewise (4), and torsional (2) loads
- Blade root edgewise load for each blade (November entry)
- Gimbal and rotor head accelerations (4)
- Pushrod loads (2)

Derived parameters calculated from the above test parameters will be discussed later in the paper.

Each of the parameters in the list above (except the Johnson-Williams LWC and the root edgewise loads) were stored on an analog tape along with a voice track, a 1-per-revolutation signal, and a time code. These parameters used 40 of the available 42 tape tracks.

Several derived parameters from the transducer outputs were computed and displayed at a rate of once per second to allow the model operator and the safety of flight (SOF) engineer to monitor loads and set target test conditions. These values accounted for tunnel blockage and buoyancy corrections, coordinate transformations, transfers, and balance interactions.

The SOF system recorded an additional 47 parameters, saved temporarily in the event of a model malfunction, but not archived for further analysis. Included on the tape were oil pressure, oil and water flow rates, drive system and motor temperatures, motor accelerations, heater voltages, limit switch and solenoid positions, rotor speed, and reference voltages.

Dynamic Data Acquisition System (DDAS)

The DDAS, safety of flight system, and model operations consoles were all located in the control room of the IRT. Data parameters were recorded on both analog and digital systems. The analog system was installed primarily as a safety of flight system and has not yet been used for data analysis. The heart of the digital system was a Digital Equipment Corporation PDP11/34 minicomputer. This test used 41 of the available 128 data channels, which were conditioned, digitized, and transferred to the PDP11 by a Neff System 620. Simultaneous sample and hold amplifiers froze the analog channels before digitizing to maintain time correlation of each parameter in each time frame (i.e., in each data snapshot). The system was configured to acquire data in both time and rotor domain. Data were acquired at a rate of 16 samples per rotor revolution during the icing test. Data acquisition hardware and software were developed to reduce the quantity of stored data, i.e., a continuous record of a 150 sec icing run with a rotor tip speed of 213.4 mps (700 fps or 37.1 Hz) would produce 3.7 million records, more than the DDAS can handle. Therefore, data were digitized only for the first 10 revolutions of each second (160 samples per data burst). The data were transferred from the DDAS to a PC/AT computer for further processing.

Safety of Flight System

Three pieces of equipment make up the model SOF instrumentation. An automated datalogger was used to monitor drive component temperatures, fluid flows and pressures, damper and balance temperatures, and various status voltages. Critical SOF parameters such as balance loads, pushrod loads, blade loads and fixed system vibrations were manually monitored during testing. Each data parameter was sent to a 42 track FM tape system which served as both an incident recorder and an analog data archive system.

Data Processing Equations

A number of commonly used rotorcraft parameters can be computed from the measured test data. An integral part of the processing of this information is the correction of the wind tunnel data for the effects of the tunnel walls. These corrections increase the effective tunnel speed and alter the rotor wake flow angles. Nondimensional terms can also be calculated to normalize the data for day-to-day changes in ambient pressure, rotor speed fluctuations, and temperature

variations. Data corrections must also be made for shaft torque tares, gravity tares, the induced angle of attack, and three-dimensional buoyancy and solid blockage effects. The coordinate systems, data correction equations, and a description of the derived parameters will be included in a future NASA Contractor Report.

TEST PROCEDURE

Test Techniques

The test techniques used in the IRT were based on previous model operating experience and procedures developed during the July to October, 1988 OH-58 tail rotor entry in the tunnel (Reference 2). Each icing run was recorded on the DDAS and video systems. The video provided a viewing history of the ice accretions and sheddings. There were three separate video systems: one for safety monitoring, one for blade tracking (which also provided good ice profile shapes near the blade tip), and one that allowed close-up images of the rotor blades. The three systems were strobe driven by a signal off the rotor shaft angle encoder. This gave a "frozen" image of the blade. The close-up data video system was installed on a tilt and pan mechanism along with a 35 mm camera that had a 400 mm zoom lens. The data video system had the capability of traversing the entire diameter of the main rotor while allowing zoom shots of as small a span as 0.10 m (3.94 in.) of the blade leading edge. The 35 mm camera was focused on the same close-up viewing area as the video camera, allowing pictures with greater resolution and clarity to be taken. Both the data video and the 35 mm camera were triggered from the same strobe to provide an accurate replication of the video image for the 35 mm camera.

During the test run, information was collected on the DDAS and the video systems, and the tunnel conditions were monitored. Liquid water content information (rise time, cloud stabilization, and spray bar lag from spray initiation) was recorded from the Control Room console output and a Johnson-Williams (J-W) LWC meter. Tables providing the main rotor operating conditions were printed out at the beginning and end of each run. Spray times, temperatures, and general comments were noted.

Post-run information was gathered by taking 35 mm camera photographs, recording ice tracings, noting visual observations, and making ice molds. Pictures were taken of the blade planform, an end profile, and any unusual ice formations. Close-up shots of ice growths were taken to record their minute detail. A heated aluminum block with a cut-out contour of the airfoil shape was used to make a clean slice through the ice formation. A template was then held against the ice shape and a tracing made. Measurements of the ice thickness along the profile were taken at various chord locations. Visual observations were recorded about the kind of ice, any secondary growth, and frost formation. Molds were taken of two blades on three separate occasions.

Test Operation

A typical test run consisted of bringing the PFM up to speed to exercise the rotor, then shutting the model down to take static balance and gage readings. The model was then brought up to operating speed and once the rotor was stabilized, a dynamic zero (wind off, zero collective) was taken. After this record the rotor rpm was dropped to some nominal level while the tunnel controls were set and the tunnel started up. When the tunnel conditions were stable the model operator returned to the desired speed, set the test point conditions, and took an uniced baseline point. The data engineer then initiated data acquisition and the tunnel operator initiated the spray sequence. At the end of the run the tunnel rpm was brought down to idle (taking approximately 2 min) while the model operator lowered the rotor speed to reduce centrifugal loads on the accreted ice. When the tunnel test section speed was below 10 kn the rotor was stopped. After the run the reseachers entered the test section and documented the results. The assembly was deiced and conditions set for the next run.

TEST DATA

Test Conditions

A total of 108 test runs were completed. Of those, 85 were icing events with the rest comprised of systems check-out, gravity and hub tares, balancing, and baselines. The test matrix was set up to include a range of conditions for a number of rotorcraft performance parameters under varied IRT conditions. For this test the temperature range was -1.7 to -29.7 °C, the LWC range was 0.35 to 1.24 g/m^3, and the MVD range was 13 to 23 μm. The predominant condition was at -15 °C, 0.50 g/m^3 LWC, and 15 μm MVD. Icing encounter times were from 54 to 168 sec. Thrust, propulsive force, advance ratio, and model rpm were changed, within the above tunnel conditions, to provide a wide scope of performance mapping.

Accuracy and Repeatability

The 2σ accuracy of the rotor loads was estimated to be:

TABLE 2. - ROTOR BALANCE ACCURACY

	Balance full scale, percent	Typical measurement, percent
Lift	0.2	1.1
Drag	.2	10
Torque	.7	2.5

The rotor head motion hardware consisted of blade pitch, flap, and lead-lag potentiometers. These potentiometers were of the single turn conductive plastic type. The total system accuracy was measured at ±0.3°.

The ability to repeat a test condition was a major goal of this test program. Rotorcraft icing flight test data has been subject to considerable data scatter, making the application of that data to code validation and basic research difficult. A portion of the observed scatter occurs due to variations in the accretion of ice on an airfoil, Reference 3, but most of the scatter comes from uncontrolled variation in the cloud. The trends from the IRT data examined show some scatter, but, in general, the data appears to be of much better quality than previous data available in the public domain. Figure 6 shows similar trends for a condition that was repeated four times. Figure 7 shows ice shape comparisons for two different repeat conditions and illustrates the small amount of variance between each of the respective runs.

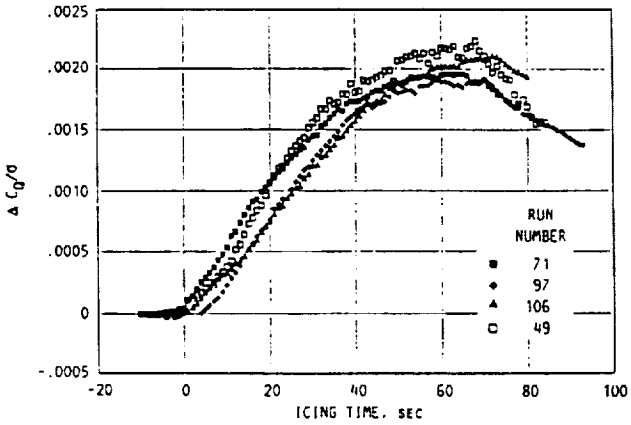

FIGURE 6. - DATA REPEATABILITY FOR FOUR REPEAT CONDITIONS (LWC = 0.50 g/m^3, MVD = 15 μm, μ = 0.20, ΩR = 206 mps, C_L/σ = 0.064, T = -15 °C).

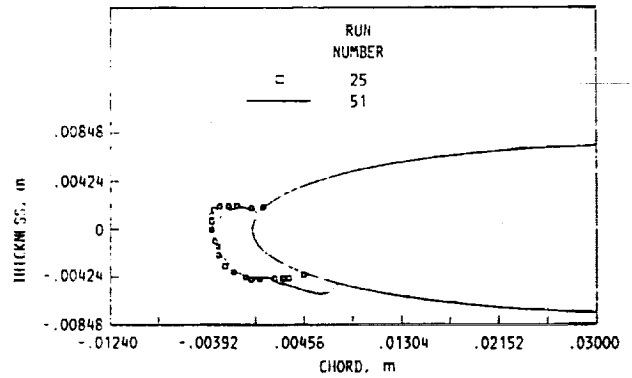

FIGURE 7. - TWO-DIMENSIONAL ICE PROFILES (LWC = 0.50 g/m^3, MVD = 15 μm, μ = 0.20, ΩR = 183 mps, C_L/σ = 0.064, T = -15 °C).

SCALING

Similarity Laws

In a test of this nature the concept of icing scaling must be addressed. Ideally, a complete scaling law must include

(1) Similarity of airflow over dry and iced surfaces
(2) Similarity of blade reaction to aerodynamic forces
(3) Similarity of droplet momentum
(4) Similarity of frozen droplet mass flux
(5) Similarity of energy balance where freezing occurs
(6) Similarity of forces which cause shedding

It should be noted that this test did not deal with scaling in a truly rigorous way. The rotor chord was about 0.127 m (5 in.) to reduce rotor chord scale effects. The tunnel geometry constrained the model to a 1.83 m (6.00 ft) diameter rotor which results in a high (0.173) solidity. A full scale version of this rotor does not exist. A number of the above scaling areas were addressed and are discussed in the following sections.

Airflow and Shedding Similarity

The main airfoil parameters are the Mach and Reynolds numbers. The model was run at full scale tip speeds because blade loading and performance were important. This simulated full scale Mach number and advance ratio. Reynolds number was considered of secondary importance because Reynolds number effects at this scale and larger are generally small and an iced airfoil transitions to turbulent flow very early. The ice/airfoil interface shear stresses (which dominate shedding characteristics) are matched at constant temperature.

Droplet Momentum

In order to simulate full scale droplet momentum it can be shown that the droplet modified inertia parameter must be kept constant. The modified inertia parameter can be expressed as

$$K_o = \frac{V^{0.62} d^{1.62}}{B^{0.38} R} \qquad (1)$$

Thus, keeping the modified inertia parameter constant and assuming total pressure and velocity are the same, the ratio of model and full scale droplet diameters can be given as

$$\frac{dm}{dF} = \left(\frac{c_m}{c_F}\right)^{0.62} \qquad (2)$$

If the modified inertia parameter is held constant the local collection efficiency will be the same for the model and full scale (Reference 4). Therefore, it would be desirable to test at very low droplet sizes, e.g., below 10 μm. The envelope of the IRT constrains the droplet size to no lower than 13 μm for the conditions tested.

Droplet Mass Flux

It has been determined that if the accumulation parameter is held constant, then the droplet mass flux which is frozen will remain constant between the model and full scale. The accumulation parameter is given as:

$$A_c = \frac{(LWC)(V)(\tau)}{\rho c} \qquad (3)$$

The derivation of the accumulation parameter assumes:

(1) Ice shape stays geometrically similar at all times.
(2) Local collection efficiency at the stagnation point is constant between model and full scale bodies.
(3) Freezing fraction at stagnation point is constant between model and full scale bodies.
(4) Shedding of any water from iced surface is zero or constant for both model and full scale bodies.

With the model's smaller chord, the icing test time needs to be kept relatively short in order to replicate a full scale icing encounter.

Energy Balance

The impinging droplets will strike the airfoil surface at geometrically similar locations as those of a full scale case if the above scaling laws are applied. However, energy balance concerns must be incorporated to assure that these droplets freeze in the same place and manner as a full scale ice shape. This is accomplished with the concept of freezing fraction, which is the ratio of frozen liquid to the total amount of liquid in a control volume and includes the impinging water as well as runback from neighboring control volumes. The general energy balance on the interfacial layer was developed by Messinger and can be found in Reference 5.

Scaling theory requires that the freezing fraction be held constant between the scaled and full scale case. This requires similarity of the heat transfer coefficient, which is strongly dependent on the surface roughness. For this test it was assumed that, after the onset of icing, the surface roughness of the ice was similar to that of full scale case. Therefore, the energy similarity was approximately satisfied.

Due to the weight constraints the blades were not dynamically scaled. It should be noted that the current state of the art scaling laws are by no means all-inclusive and much work is needed in this area. Several shortcomings of the similarity laws are evident. First, the mass and energy balance do not include the effects of movement and shedding of water on the surface as well as ice shedding. Further, the basic assumptions from which the ice accretion energy balance was derived have recently been shown to be in error. Films have shown that there is a distinct multizonal characteristic to airfoil ice accretion (Reference 6). The traditional runback model appears to be valid in the region near the stagnation point. Here, the energy balance described above would be appropriate. However, in the region aft of the transition point, which would include the majority of the region of accretion, surface tension forces appear to dominate and little or no runback occurs. Thus, more work leading to a modified similarity law is needed in this area. It was felt that, given the constraints of the project that similarity was met to the highest possible degree for this rotor. There is a great deal of confidence that the data taken is valid for analysis purposes. Future validation of this test technique however, would dictate that a model rotor with a full scale equivalent be chosen.

DATA ANALYSIS AND CORRELATION

Data Initialization

The data has been reviewed to determine experimentally the onset of icing. The establishment of this onset was based on a Johnson-Williams LWC probe data when available, as well as the change in rotor torque and lift. This approach has been used throughout the analysis for the preparation of parameter comparisons.

Liquid Water Content

The liquid water content and droplet diameter of the spray cloud are dependent on the spray bar water and air pressures, and the tunnel velocity. The pressure values are generated from a set of calibration equations. The above approach gives an accurate setting for LWC, but it does not provide any history of the spray which is necessary to understand the cloud time lag between spray on and model inundation, rise time to the target LWC, and cloud characteristic during the spray. A Johnson-Williams (J-W) liquid water content meter was installed slightly in front of and below the rotor. This provided cloud information to detail the above concerns.

The duration of the sprays ranged from 54 to 186 sec. Scale rotor testing must use these shorter times to replicate full scale conditions. However, this presents some concern in the IRT because these short spray durations fall within the spray stabilization time, i.e., it normally takes up to a minute for the cloud to reach steady state condition. A plot of the J-W LWC data for a number of runs (Figure 8) indicates that there is some rise time prior to reaching the target value (with the rise time increasing at the higher LWC runs), but the spray condition remains relatively close to the desired setting after the ramp up. The cloud reached the model about 10 sec after the "spray

on" command was given. The LWC repeatability is shown for two different spray bar settings in Figure 9.

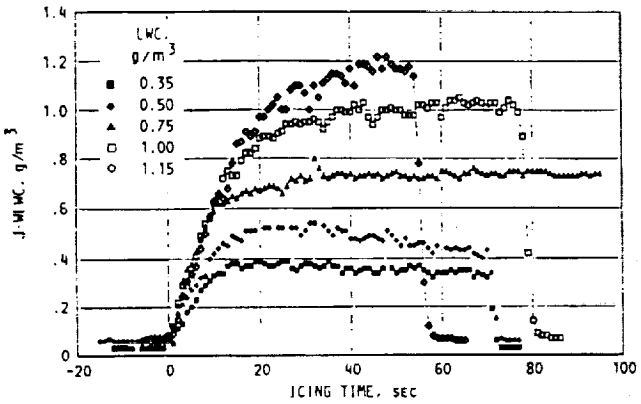

FIGURE 8. - VARIOUS LWC RUNS VERSUS ICING TIME (MVD = 15 μm, μ = 0.20, ΩR = 206 mps, C_L = 0.064, T = -15 °C).

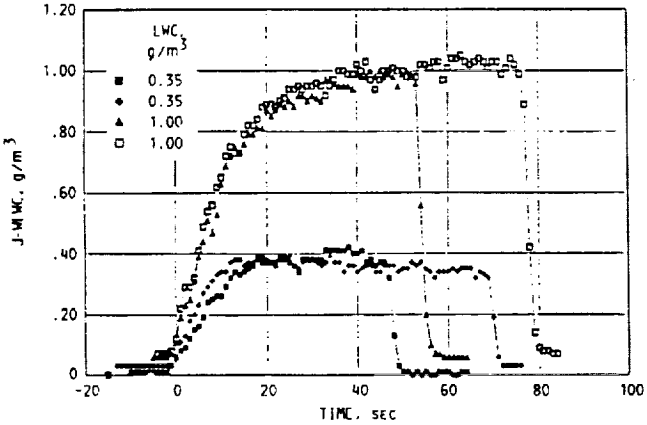

FIGURE 9. - LWC REPEATABILITY VERSUS ICING TIME (MVD = 15 μm, μ = 0.20, ΩR = 206 mps, C_L/σ = 0.064, T = -15 °C).

The data follows expected trends when the LWC is increased. The torque data shows an increase (Figure 10) and the lift performance degrades (Figure 11).

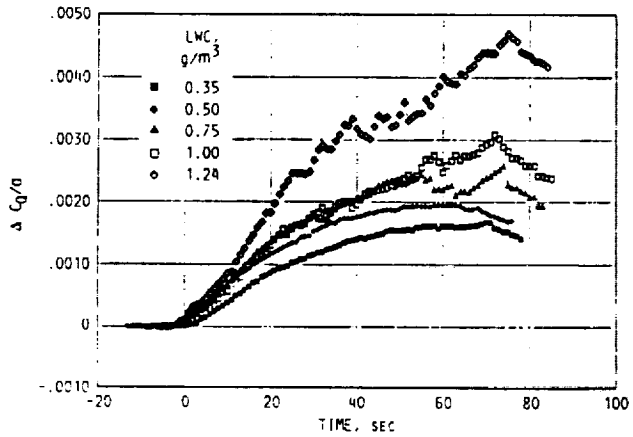

FIGURE 10. - LWC EFFECT FOR Δ C_Q/σ VERSUS ICING TIME (MVD = 15 μm, μ = 0.20, ΩR = 206 mps, C_L/σ = 0.064, T = -15 °C).

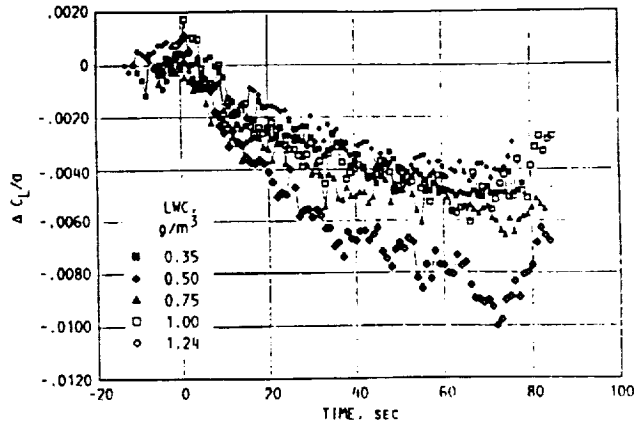

FIGURE 11. - LWC EFFECTS FOR Δ C_L/σ VERSUS ICING TIME (MVD = 15 μm, μ = 0.20, ΩR = 206 mps, C_L/σ = 0.064, T = -15 °C).

The median volume droplet diameter was changed in a range from 13 to 23 μm at a constant LWC of 0.75 g/m^3. The results indicate that an increase in MVD size has the expected effect of increasing the torque (Figure 12). The droplet diameter has no significant effect on lift for the range of MVD sizes tested. There was good repeatability for the 13 and 15 μm cases, but the results are less clear with the 18 and 23 μm sizes.

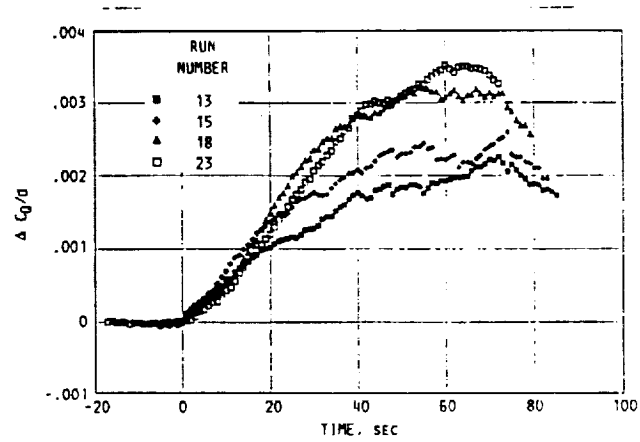

FIGURE 12. - MVD EFFECTS FOR Δ C_Q/σ VERSUS ICING TIME (LWC = 0.50 g/m^3, μ = 0.20, ΩR = 206 mps, C_L/σ = 0.064, T = -15 °C).

Delta Lift And Torque Trends

The precision of the balance made the accuracy of X bar less than desired. The balance, which was sized to accommodate the vibratory loads due to ice shedding, was too large to measure precisely the low drag loads at the primary test speed of 31.1 m/sec (80 kn). However, the data show that shaft angle, and hence X bar, are of secondary importance in the data trends (Figure 13). Therefore, small differences in X bar are not significant, and data comparisons are made with runs that have similar but not identical values.

The test was generally done with the collective pitch and shaft angle held constant during the icing encounter. For most of the trends

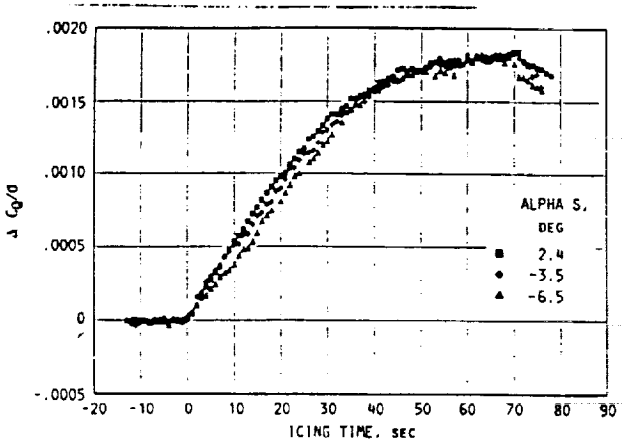

FIGURE 13. - SHAFT ANGLE EFFECTS ON TORQUE (LWC = 0.50 g/m^3, MVD = 15 μm, μ = 0.20, ΩR = 206 mps, C_L/σ = 0.064, T = -15 °C.

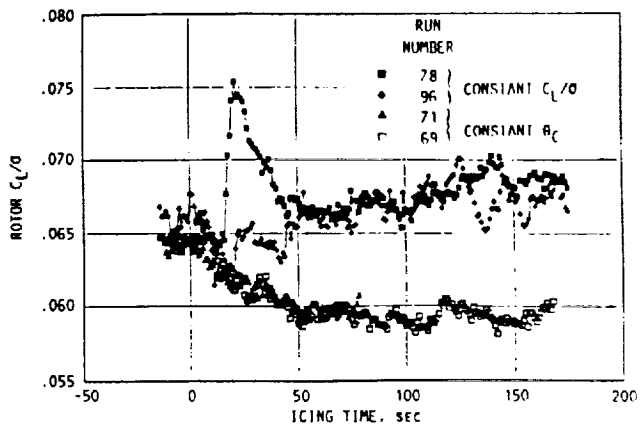

FIGURE 15. - EFFECT OF HOLDING LIFT CONSTANT FOR C_L/σ VERSUS TIME (LWC = 0.50 g/m^3, MVD = 15 μm, μ = 0.20, ΩR = 206 mps, C_L/σ = 0.064, T = -15 °C).

shown in this report the initial C_L/σ was about 0.065 and the initial C_Q/σ was about 0.0047. However, many theoretical comparisons may be better performed at constant lift conditions. Therefore, three conditions were repeated with the model pilot maintaining zero flapping and C_L/σ at the initial value. The transient nature of icing creates a significant pilot workload, but the results show that the condition can be flown, and that changes in collective during the run have an impact on the data. Figure 14 shows the power increases for this constant lift case and Figure 15 shows the lift history. Collective increased about 0.5° for these cases.

Temperature was varied from near freezing to very cold (-30.5 °C). Figure 16 shows a plot of the power increase for temperatures ranging from -3.7 to -15.2°. The torque increases as temperature decreases because, in this temperature range, the radial icing extent increases. As more of the rotor blade is iced the performance penalties become more severe. Figure 17 shows another plot of torque rise for a much colder temperature range, -15.2 to -30.5 °C. Here, the torque rise trend reverses and actually decreases with temperature. As the temperature decreases the ice shape changes from glaze to rime, and the performance penalties are less.

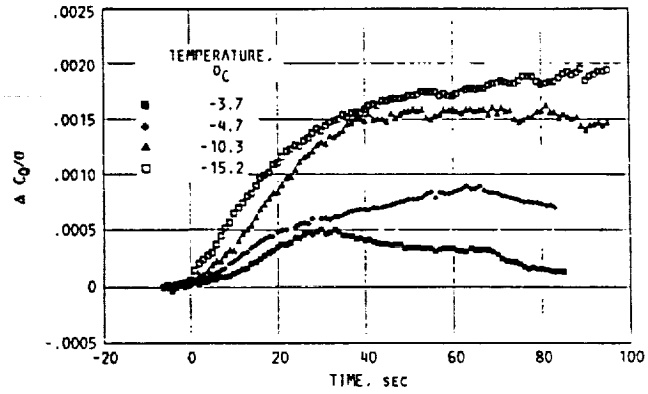

FIGURE 16. - TEMPERATURE EFFECTS FOR Δ C_Q/σ VERSUS ICING TIME (LWC = 0.50 g/m^3, MVD = 15 μm, μ = 0.20, ΩR = 206 mps, C_L/σ = 0.064).

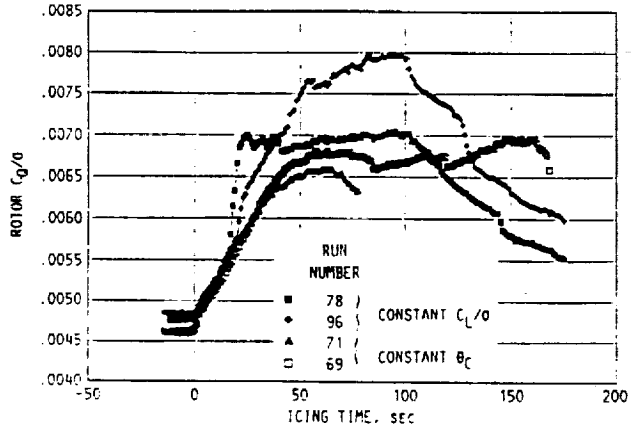

FIGURE 14. - EFFECT OF HOLDING LIFT CONSTANT FOR C_Q/σ VERSUS TIME (LWC = 0.50 g/m^3, MVD = 15 μm, μ = 0.20, ΩR = 206 mps, C_L/σ = 0.064, T = -15 °C).

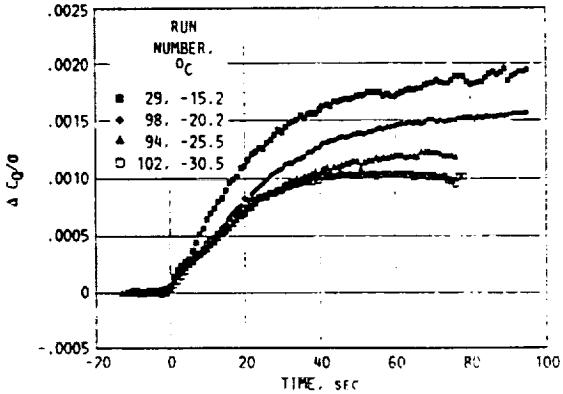

FIGURE 17. - TEMPERATURE EFFECTS FOR Δ C_Q/σ VERSUS ICING TIME (LWC = 0.50 g/m^3, MVD = 15 μm, μ = 0.20, R = 206 mps, C_L/σ = 0.064).

Figure 18 shows a plot of the lift loss for the entire range of temperatures. The trend is consistent with that of the torque, except for the extremely cold temperature (-30.5 °C).

The effects of icing on rotor torque at different tip speeds is shown in Figure 19. There appears to be a critical velocity between 152 and 183 mps. For the former case the torque rise steadily increases throughout most of the run. However, the roll-off and maximum values for the three higher speed cases is roughly the same. For the higher tip speeds a balance between shedding and accretion appears to have been reached such that the torque levels off after roughly 50 sec of icing time.

Although data were taken for sweeps of advance ratio and disk loading at this time there is not enough evidence to support any conclusive remarks in these areas. These topics will be addressed in detail once a thorough analysis of the data is completed.

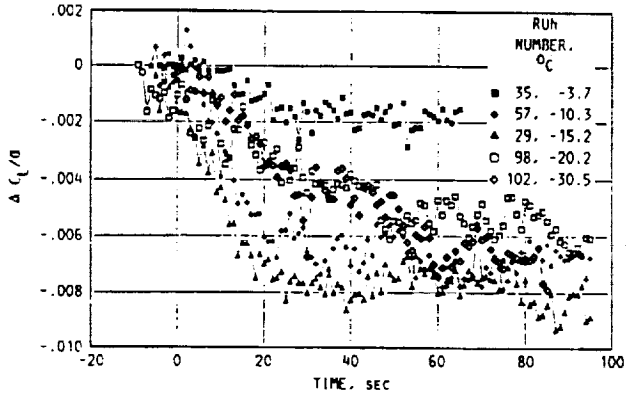

FIGURE 18. - TEMPERATURE EFFECTS FOR Δ C_L/σ VERSUS ICING TIME (LWC = 0.50 g/m^3, MVD = 15 μm, μ = 0.20, ΩR = 206 mps, C_L/σ = 0.064).

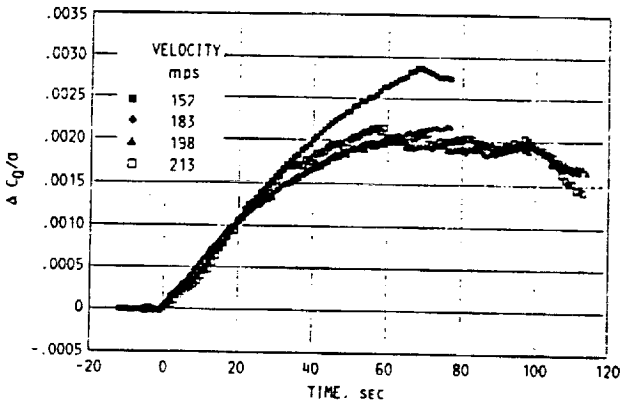

FIGURE 19. - TIP SPEED EFFECTS FOR Δ C_Q/σ VERSUS ICING TIME (LWC = 0.50 g/m^3, MVD = 15 μm, μ = 0.20, C_L/σ = 0.064, T = -15 °C).

Accretion

Fundamental to any simulation of an icing encounter is the correct representation of the accreted ice shape. If accurate data on performance degradation is desired, a model icing experiment must accrete ice in a manner similar to full scale flight. An assessment of the quality of the data must begin with an evaluation of the correctness of the accreted ice shapes in terms of repeatability and trends. Repeatability has been established in an earlier section; a discussion of the trends will follow.

A helicopter rotor blade will experience nonuniform ice growth as a function of radial location due to the velocity variation and the attendant aerodynamic heating effects along the span of the blade. The local rime ice growth is dependent on the Accumulation Parameter which is a function of velocity, and as velocity increases the overall thickness of the resulting ice shape will increase. Also, as velocity increases the effects of aerodynamic heating become important and raise the surface temperature to a point where rime transitions to glaze. These trends are born out in Figure 20 which shows the radial variation of accretion for a typical run. The primary shape increases in size from the 50 percent to the 70 percent spanwise location, and the ice profile changes from a smooth rime shape at the 50 percent location to a rough glaze shape at the 90 percent location.

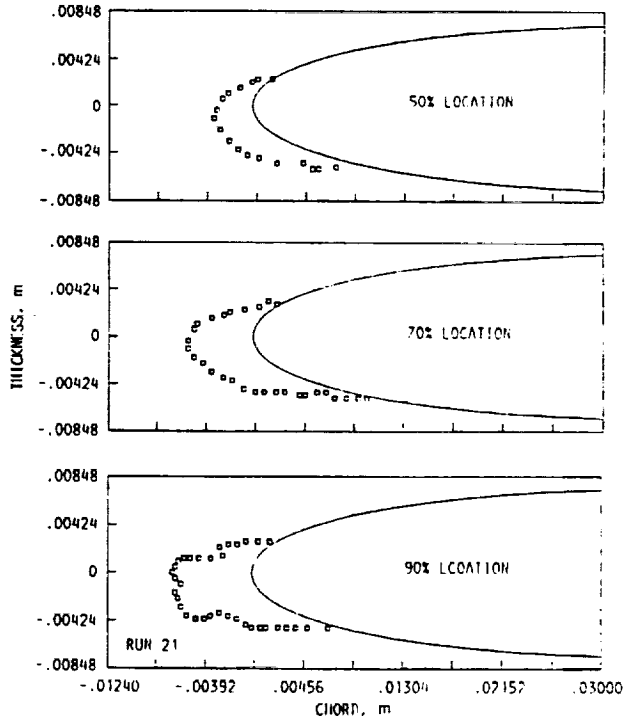

FIGURE 20. - RADIAL VARIATION OF ICE SHAPE (LWC = 0.50 g/m^3, MVD = 15 μm, μ = 0.20, ΩR = 213 mps, C_L/σ = 0.046, T = -25 °C).

The accretion characteristics are also determined by the droplet size and the liquid water content. Rime ice tends to be associated with smaller droplets and glaze ice with larger ones. Figure 21 illustrates this by showing the transition from a rime shape for 13 μm to a rougher glaze shape for 18 μm. The figure also shows that the lower impingement limit moves back as the droplet size increases. The smaller particles, with lower inertia parameters, are more likely to be deflected around the airfoil resulting in a narrow collection zone close to the stagnation point (Reference 7). As the particle size increases the inertia parmeter increases and the droplets are less influenced by the airfoil flowfield, striking the surface further aft of the stagnation point. The liquid water content is a measure of how much moisture is in the cloud; the higher the liquid water content, the more severe the icing encounter. As shown in Equation (3) for rime ice, the thickness of the ice is linearly proportional to the liquid water content. This can be seen in Figure 22 which shows an increase in ice thickness for increasing liquid water content.

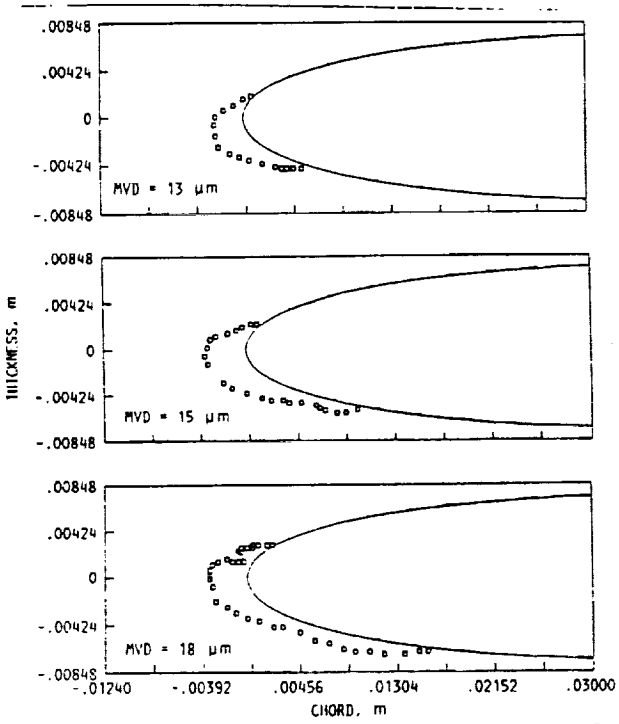

FIGURE 21. - ICE SHAPES FOR VARIOUS MVD'S (LWC = 0.50 g/m^3, μ = 0.20, ΩR = 206 mps, C_L/σ = 0.064, T = -15 °C, r/R = 50%).

The ability to adequately predict a given ice shape is critical to a rigorous methodology which predicts performance degradation during an icing encounter. The current state of the art in this area is the computer analysis LEWICE, which was developed at NASA Lewis. LEWICE is a two-dimensional code which, given the geometric and atmospheric conditions, will predict the cross-sectional ice shape for a specified icing time. Several comparisons have been made between the predictions of LEWICE and this experimental data. The local angle of attack

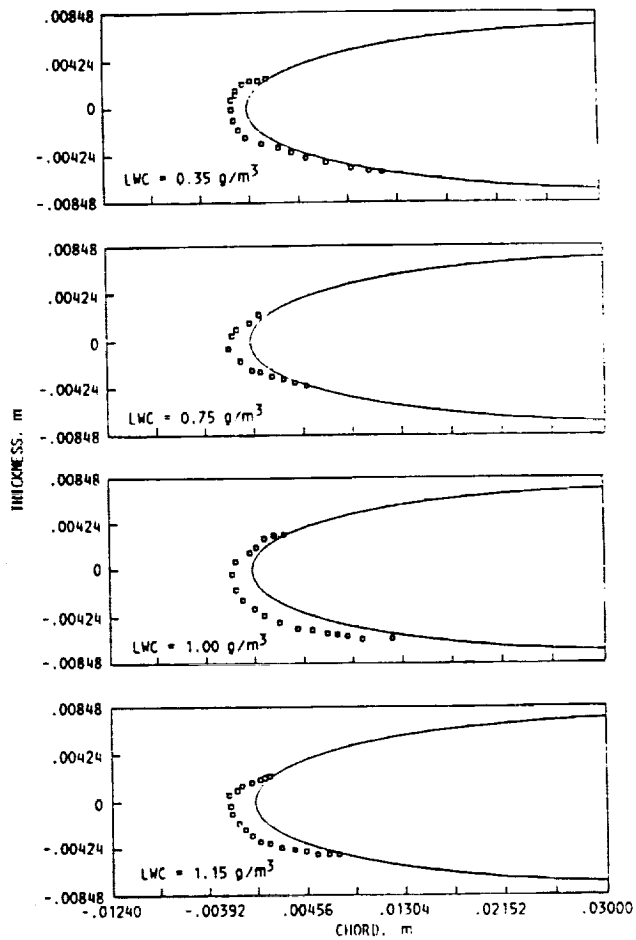

FIGURE 22. - ICE SHAPES FOR VARIOUS LWC'S (MVD = 15 μm μ = 0.20, ΩR = 206 mps, C_L/σ = 0.064, T = -15 °C, r/R = 50%).

was determined with the Boeing Helicopter B65 computer performance code. The Mach number and angle of attack were azimuthally averaged for input into LEWICE, as shown to be appropriate by Korkan, Dadone, and Shaw (Reference 8). The guidelines for time step size and surface roughness were those described by Korkan and Britton (Figure 9). Figure 23 shows two sample comparisons for a rime condition. The overall aggreement is good with slight overprediction by LEWICE on the lower surface. The majority of comparisons made to date have been for rime conditions and the preliminary results have been encouraging.

In any experiment of this type it is important to establish the quality of the accretion data because it is fundamental to the confidence in the rest of the experimental information. The preliminary evidence indicates that the ice accretion data is repeatable and follows the correct trends. Any substantial quantitative statement about the quality of the data will have to wait until a full analysis can be completed.

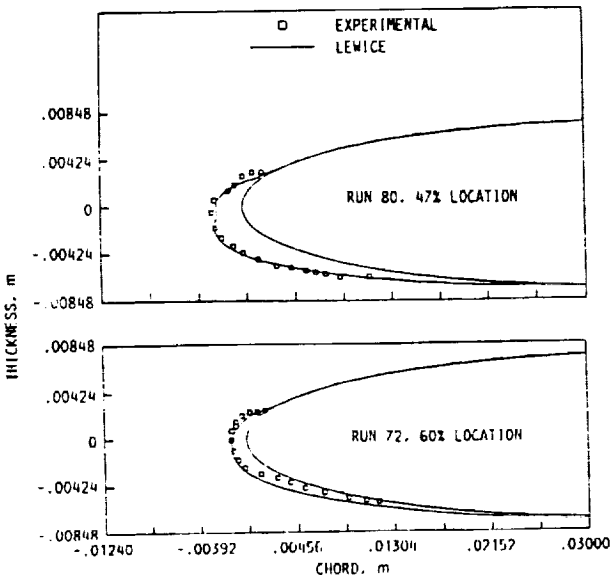

FIGURE 23. - COMPARISON BETWEEN EXPERIMENTAL AND THEORETICAL ICE SHAPES (LWC = 1.00 g/m^3, MVD = 15 μm, μ = 0.20, ΩR = 206 mps, C_L/σ = 0.064, T = -15 °C).

Shedding

The ice shedding process is a important factor in a propeller or rotorcraft icing encounter; this phenomena dominates the outcome of the entire icing event. The shedding process is influenced by centrifugal forces, aerodynamic loading, and the elastic deformations of the blades. Shedding can pose several potential problems for rotorcraft. The ice leaving the blades at high tip speeds has substantial energy and can cause fuselage damage for rotorcraft, especially tilt-rotor and propeller applications. Also, when ice sheds in a nonuniform fashion an out-of-balance condition can arise resulting in high vibratory loads.

Figure 24 shows a plot of the root strain gage output for each of the blades as a function of time. When a shed occurs there is a large fluctuation in the strain gage reading. There were two major shedding events for this run; one at approximately 25 sec and another at about 38 sec. For both events blade number 4 experiences a shed first, followed by sheds from the other blades. Rotor torque, also shown in Figure 24, exhibits a small reduction in torque during minor shedding, with more pronounced changes in torque at major shedding events. There were instances where ice was shed asymmetrically, but the model vibration load limits were not exceeded. Figure 25 shows an example of a section of a blade with ice shed. While this shows a relatively clean break in the ice, the majority of the time there is some residual ice left on the blade after a shed.

A preliminary viewing of the high speed movies found nine ice shed events either partially or completely captured. It is hoped that this information, along with the shed impact data can be used to validate an ice shedding computer model currently being developed.

The condition of the blade surface has an effect on shedding characteristics. While the blades and exposed areas of the hub were wiped clean of any bearing grease prior to every run, post run examination revealed some degree of grease on the inboard portions of the airfoil leading edge. The effects on adhesion properties are not known, but the data examined show that ice shedding was reasonably repeatable.

Correlation With Theory

The current work in analytical modeling has been a preliminary investigation of ice accretion (shown in Figure 19). We will continue to correlate the experimental data with the B65 and Sikorsky GRP forward flight performance codes, and the LEWICE accretion code.

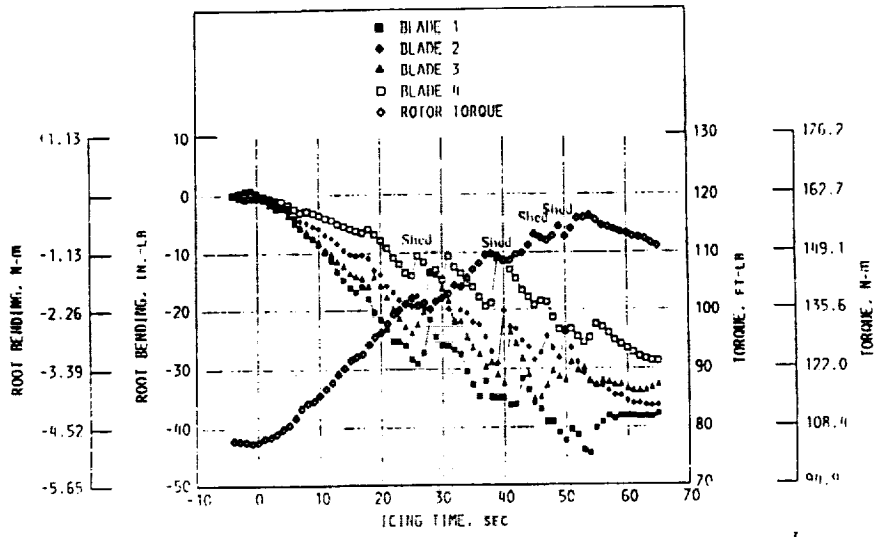

FIGURE 24. - BLADE ROOT BENDING AND TORQUE RISE VERSUS ICING TIME (LWC = 1.00 g/m^3, MVD = 15 μm, μ = 0.20, ΩR = 206 mps, C_L/σ = 0.064, T = -15 °C).

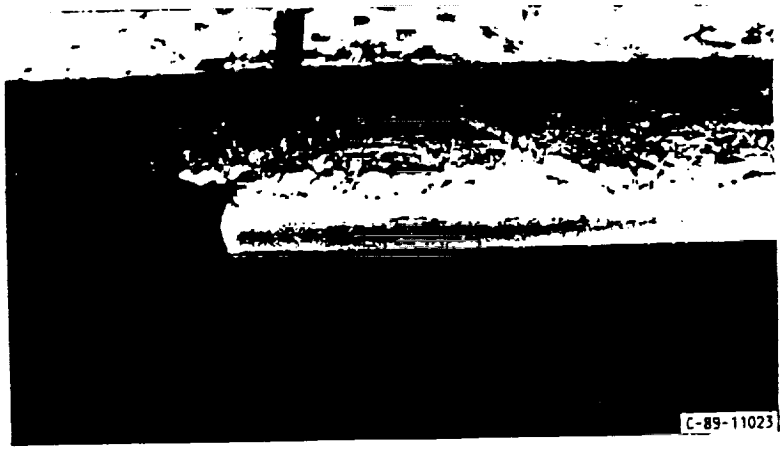

FIGURE 25. - CLOSE-UP DETAIL OF ICE SHED.

CONCLUSIONS

Concluding Remarks

The examination of the data from the PFM testing has provided encouraging results. The quality of the test data appears to be excellent. The changes in lift and torque are well documented and are remarkably repeatable. The model instrumentation clearly shows the time of shedding events and templates have been made to document the ice shapes at the end of each test run.

The data show the effects of temperature, rpm, liquid water content, and droplet diameter on icing. The qualitative trends of the data reviewed to date are correct and the test process looks sound. The lift at a constant control collective dropped by up to 15 percent. Torque increases of 50 percent and more were common. It appears that the techniques employed have been validated by the results obtained, and that the data will be useful for code and scaling research and development.

Future Plans

The near term goal is the completion of the data analysis for the PFM entries. We will continue the examination of the rotor performance data. Only a small amount of the ice accretion and shedding data have been reviewed. Correlation studies will be done to see if new empirical equations need or can be developed. High speed 16 mm movies will be processed, and this information used with the energy impact data to support ice accretion and shedding model development. The molds taken during the testing will be used to make ice castings and hopefully these will have the quality needed for ice simulation experiments.

The longer term goals include further model icing tests, coordinated with full-scale rotorcraft icing flight testing. This would follow a logical progression for development and verification of the model rotor test techniques and the analytical methods, and identify where their use in main rotor design is appropriate.

ACKNOWLEDGEMENTS

It took the efforts of all the consortium members to make this test successful possible. The authors wish to thank all those involved throughout the development of this project, in particular the NASA IRT Test Installations Division personnel and Sikorsky Aircraft Experimental Aeromechanics Section model operators.

REFERENCES

1. Guffond, D.P., "Icing and De-Icing Test on a 1/4 Scale Rotor in the ONERA SIMA Wind Tunnel," AIAA Paper 86-0480, Jan. 1986.

2. Miller, T.L. and Bond, T.H., "Icing Research Tunnel Test of a Model Helicopter Rotor," NASA TM-101978, 1989.

3. Flemming, R.J. and Lednicer, D.A., "High Speed Ice Accretion on Rotorcraft Airfoils," NASA CR-3910, 1985.

4. Olsen, W., Takeuchi, D., and Adams, K., "Experimental Comparison of Icing Cloud Instruments," AIAA Paper 83-0026, Jan. 1983 (NASA TM-83340).

5. Messinger, B.L., "Equilibrium Temperature of an Unheated Icing Surface As a Function of Airspeed," J. Aeronaut. Sci., vol. 20, no. 1, Jan. 1953, pp. 29-42.

6. Olsen, W.A., Warther, E.D., and Sotos, R.G., "Microscopic High Speed Movies Shwoing the Droplet Freezing Process of Icing," AIAA Paper 84-0019, Jan. 1984.

7. Britton, R.K., "Elevator Deflection Effects on The Icing Process," AIAA Paper 89-0846, Jan. 1989.

8. Korkan, K.D., Shaw, R.J., and Dadone, L., "Performance Degradation of Helicopter Rotor Systems in Forward Flight Due to Rime Ice Accretion," AIAA Paper 83-0029, Jan. 1983.

9. Korkan, K.D. and Britton, R.K., "Ice Shape Prediction Methodology and Comparison With Experimental Data," AIAA Paper 90-0753, Jan. 1990.

Appendix C

Photo No.	Run No.	LWC (g/m^3)	VMD μ	Time (sec)
C-90-02358	80	0.98	15	54
-02360	76	0.7	15	200
-02362	76	0.7	15	200
-02363	76	0.7	15	200
-02364	76	0.7	15	200
-02365	76	0.7	15	200
-02366	76	0.7	15	200
-02367	76	0.7	15	200
-02370	71	0.43	15	80
-02371	73	0.38	15	80
-02372	71	0.43	15	80
-02374	69	0.5	15	168
-02375	70	0.5	15	54
-02378	69	0.5	15	168
-02384	76	0.7	15	200
-02391	100	1.00	15	80
-02393	94	0.5	15	80
-02400	90	0.74	13	168
-02401	85	0.74	23	80
-02403	85	0.81	18	80
-02405	80	0.98	15	54
-02553	47	0.5	15	80

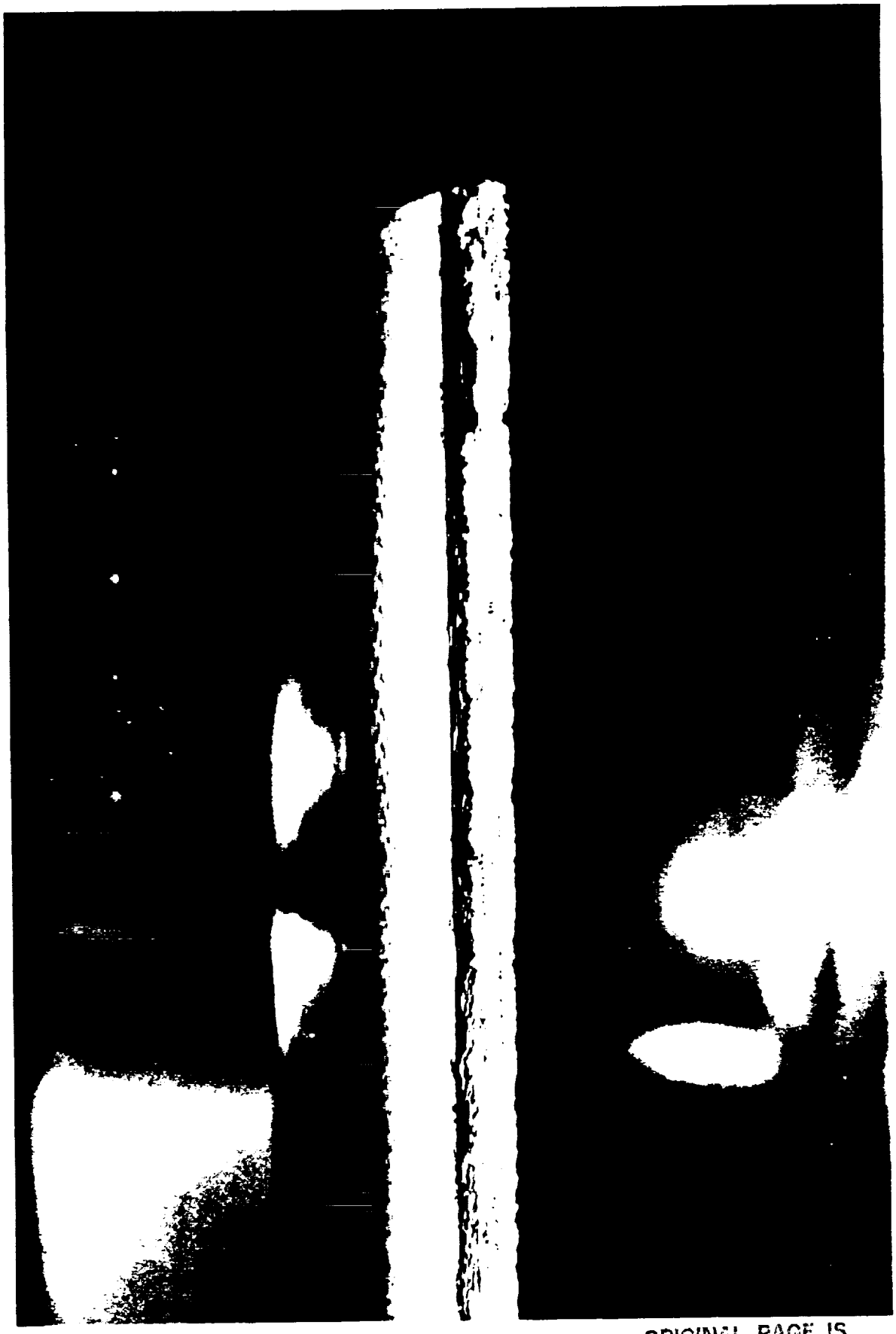

C-90-02553

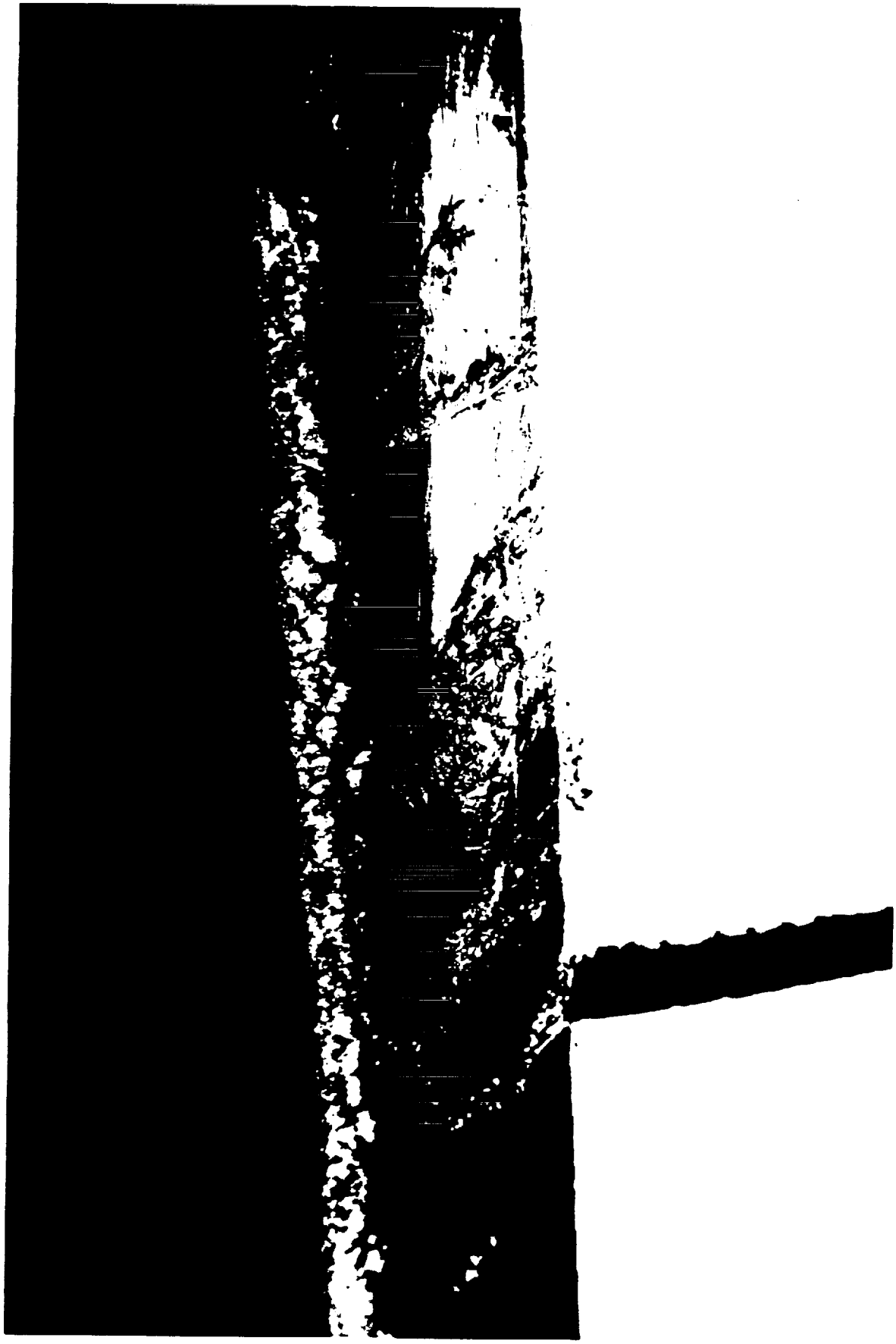

NASA
C-90-02358

ORIGINAL PAGE IS
OF POOR QUALITY

C-90-8240

ORIGINAL PAGE IS
OF POOR QUALITY

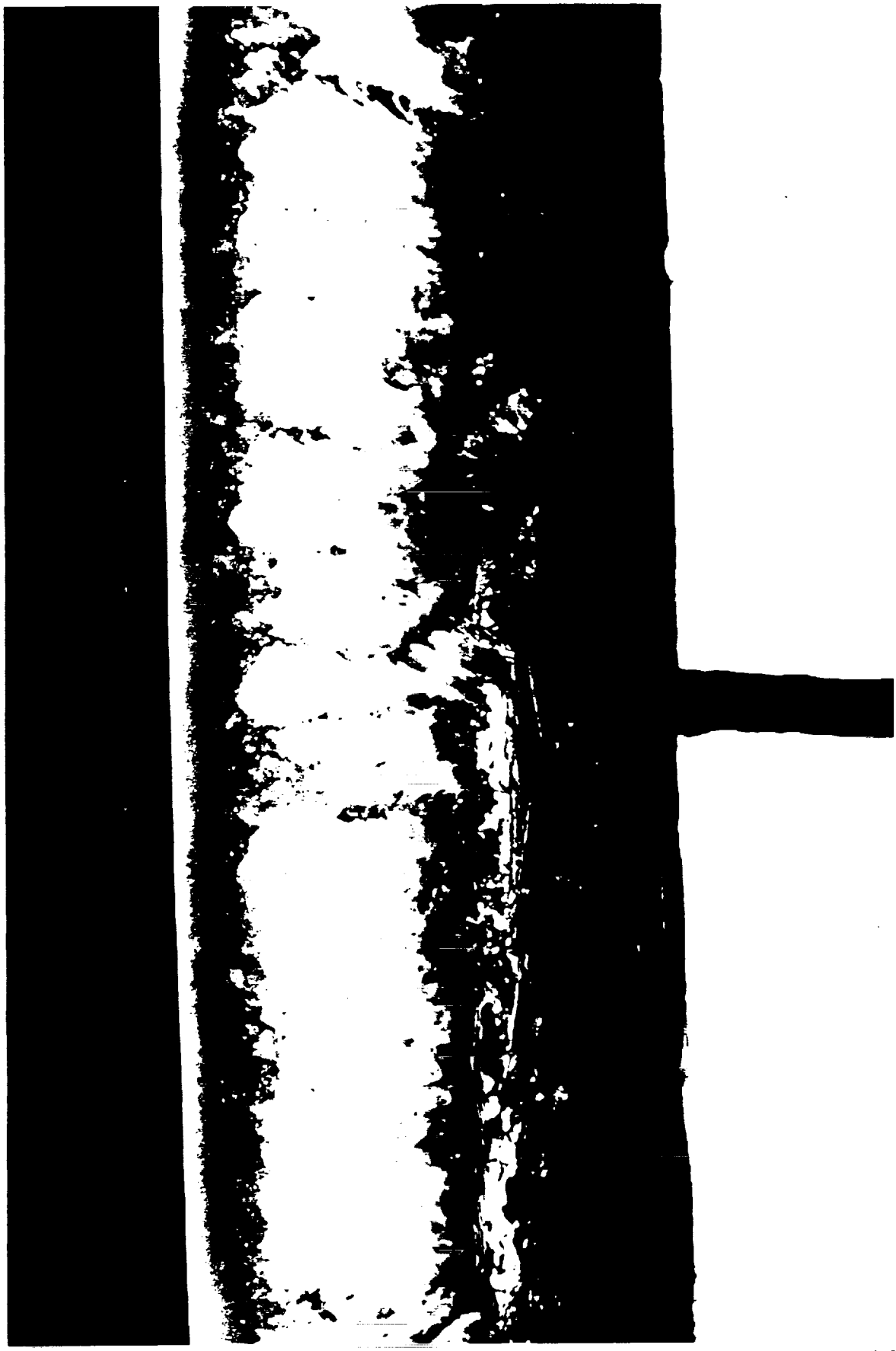

NASA
C-90-02362

C-90-02364

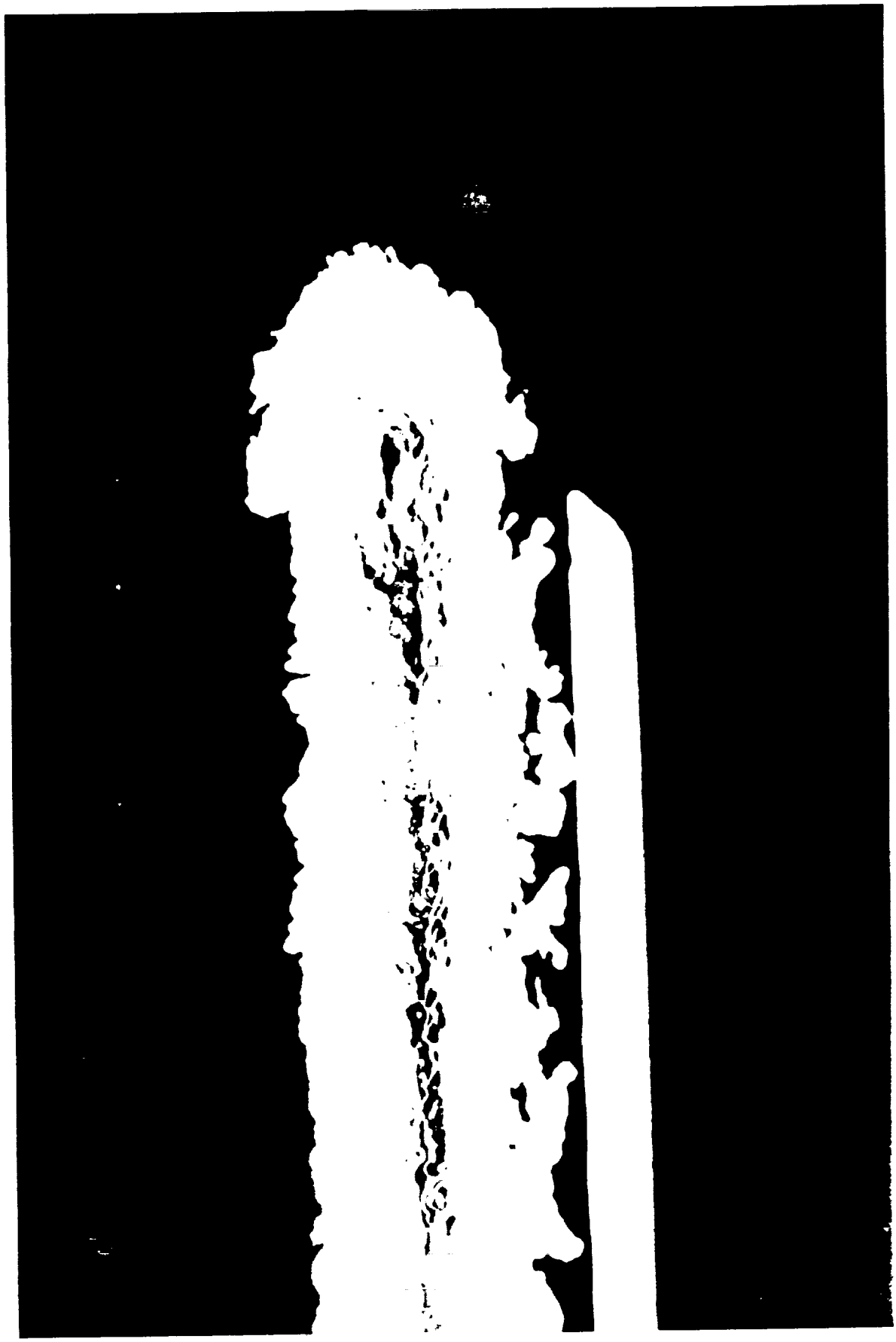

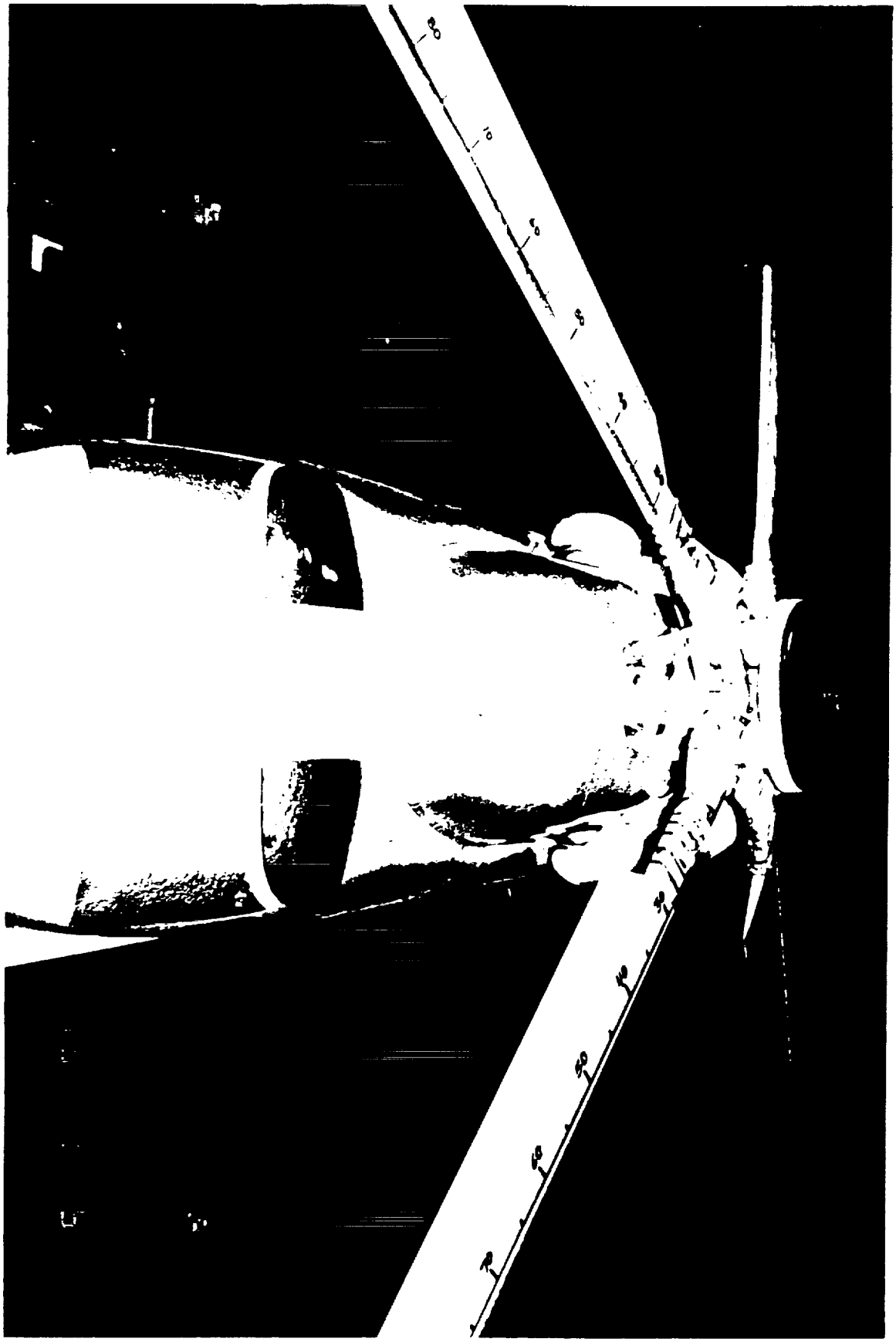

C-90-02366

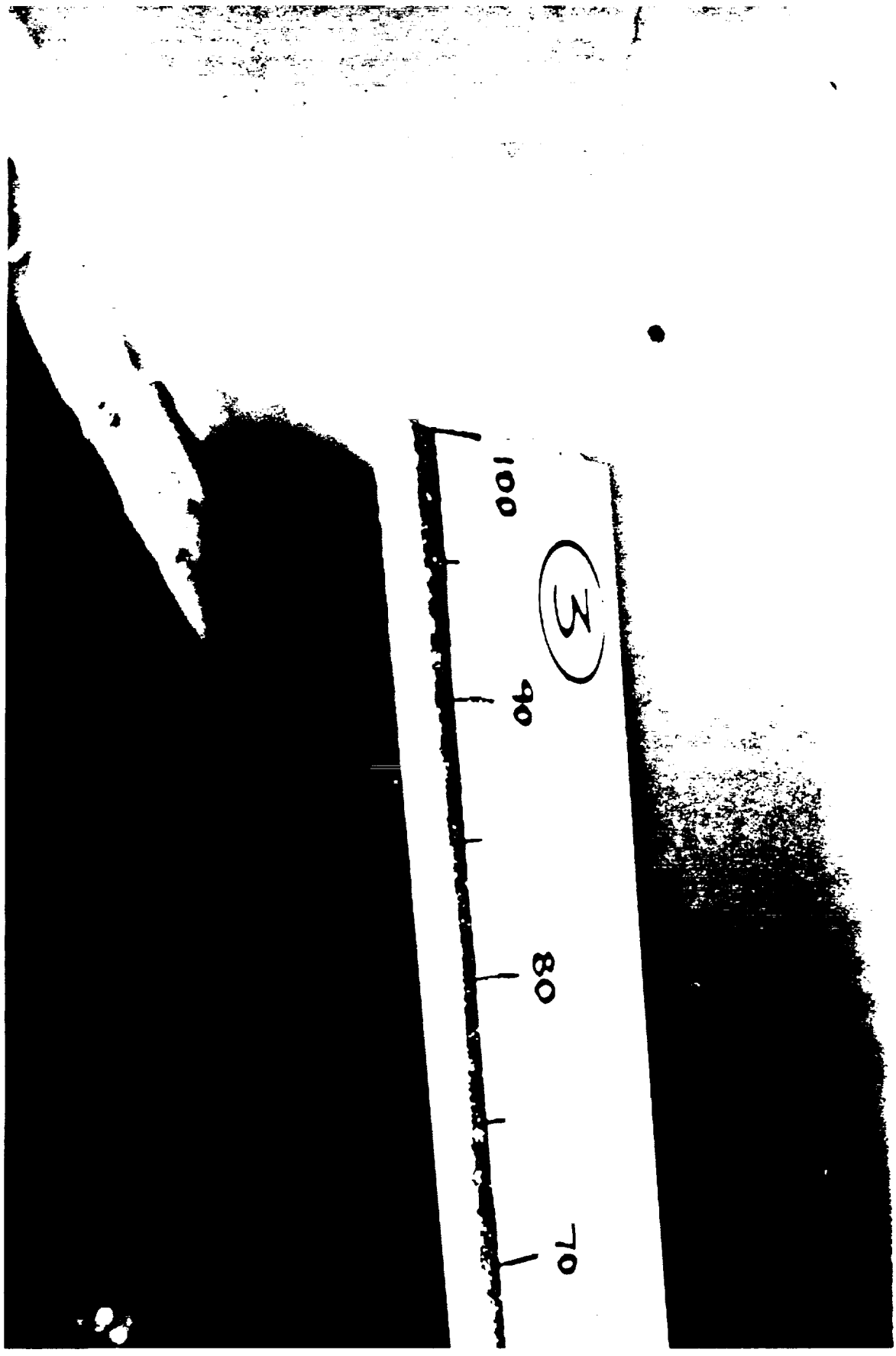

C-88-02370

NASA
C-90-02371

C-90-02572

ORIGINAL PAGE IS
OF POOR QUALITY

C-90-02375

ORIGINAL PAGE IS
OF POOR QUALITY

C-90-02378

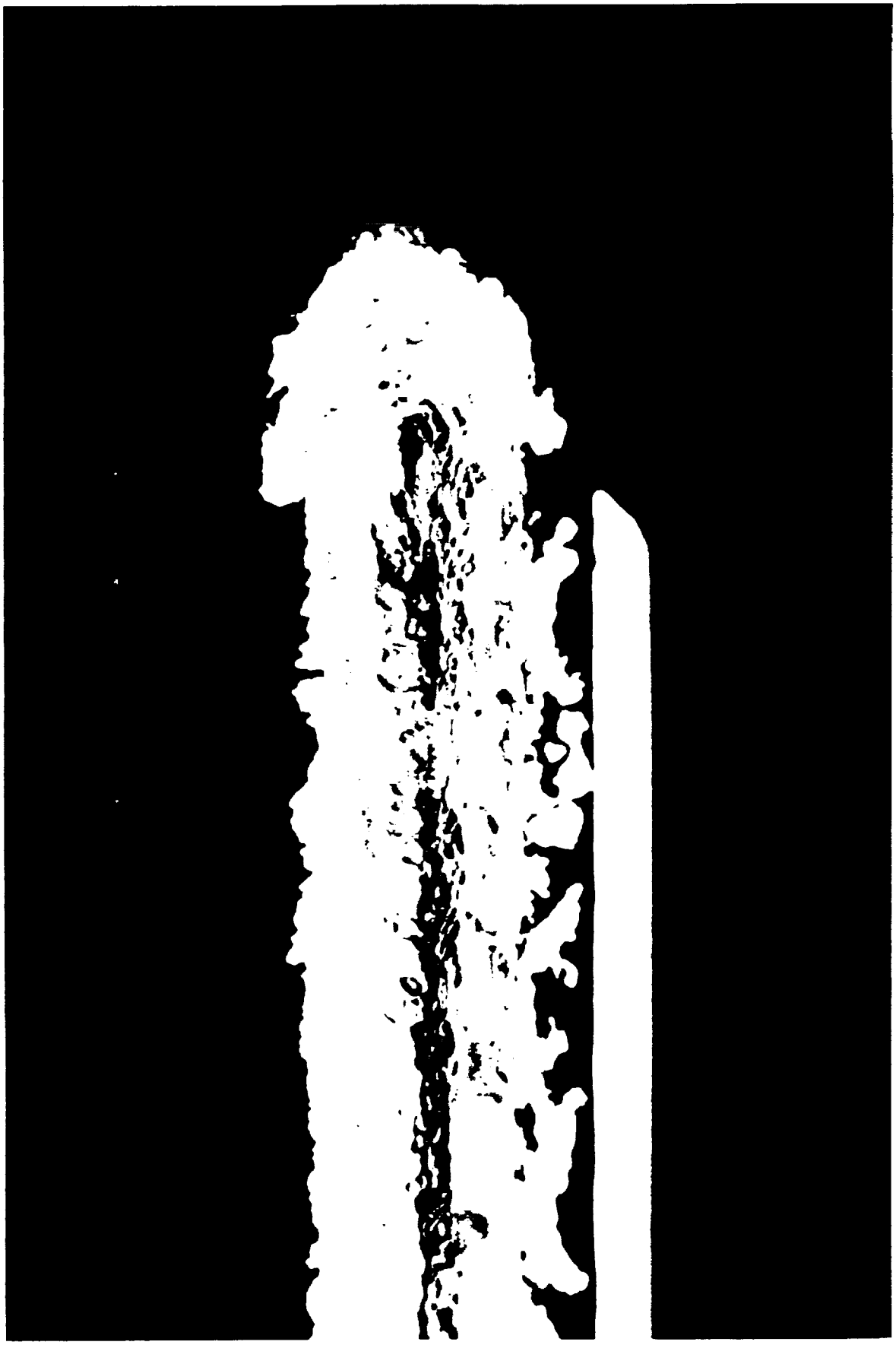

ORIGINAL PAGE IS
OF POOR QUALITY

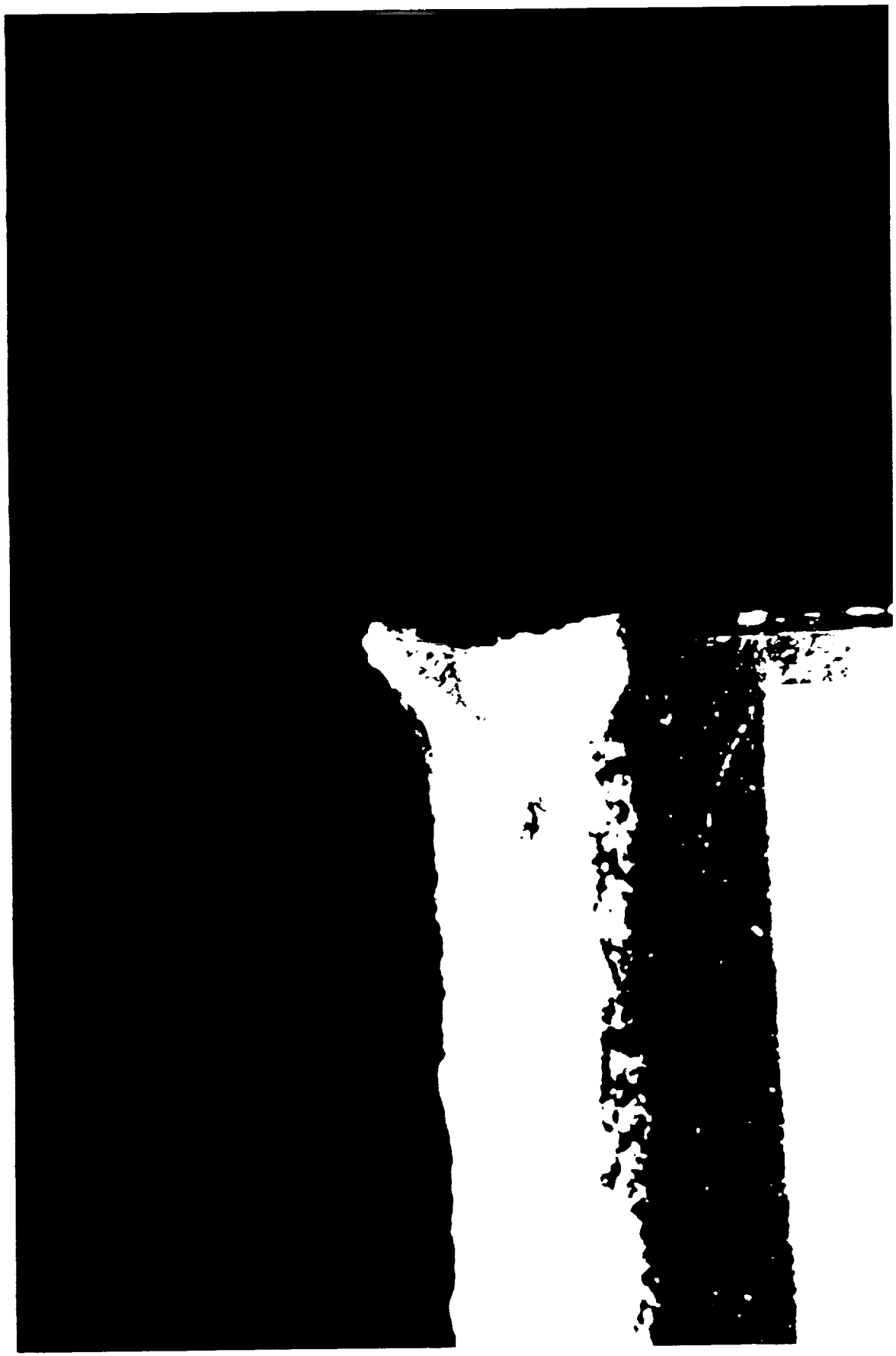

NASA
C-90-02391

NASA
C-90-02393

ORIGINAL PAGE IS
OF POOR QUALITY

NASA
C-90-02400

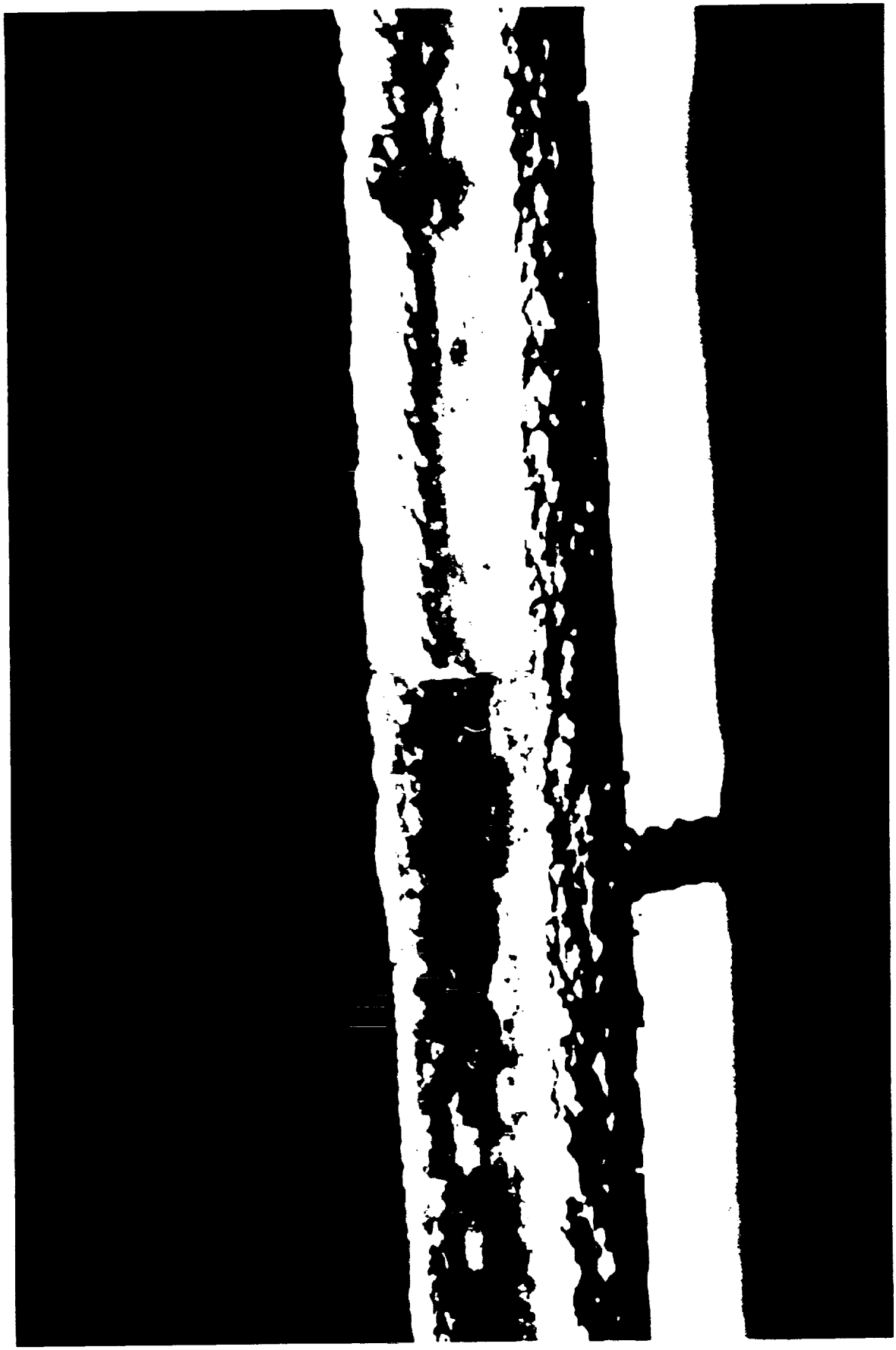

NASA
C-90-02403

ORIGINAL PAGE IS
OF POOR QUALITY

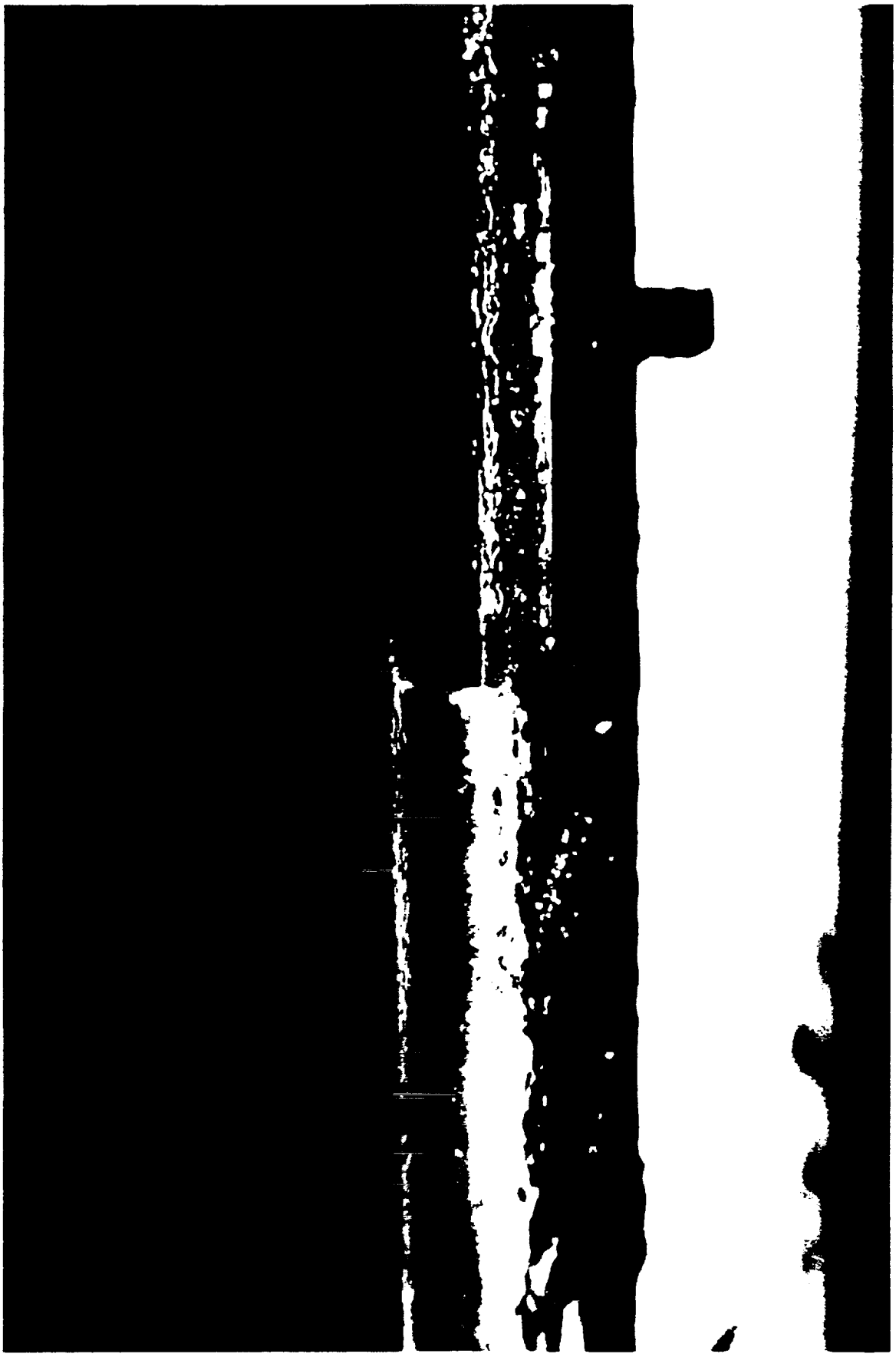

NASA
C-90-02405

ORIGINAL PAGE IS
OF POOR QUALITY